Future developments in surge forecast: probabilistic forecast and future surge statistic

Riccardo Mel

This thesis is presented for the degree of Doctor of Civil and Environmental Engineering Science University of Padova

Department of Civil, Architectural and Environmental Engineering (DICEA) University of Padova

2013

Abstract

This research investigated how the surge forecast can be improved, moving from a single-deterministic to a probabilistic forecast. Moreover a future storm surge scenario is estimated using new meteorological data: sea level (SL) forecast for the city of Venice and future changes of storm surge regime due to climate changes are of paramount importance for the management and maintenance of this historical city and for operating the movable barriers that are presently being built for its protection.

An Ensemble Prediction System (EPS) for operational forecasting of storm surge in the northern Adriatic Sea is presented. EPS is meant to complement the existing SL forecast system by providing a probabilistic forecast and information on uncertainty of SL prediction. Ten relatively high storm surge events in the period 2009-2010 are simulated producing for each of them an ensemble of 50 simulations, using the meteorological data input of the European Centre for Medium-Range Weather Forecasts (ECMWF) as input to a shallow water hydrodynamic model "Hydrostatic Padua Surface Elevation Model" (HYPSE), which computes sea level and barotropic currents in the Adriatic Sea . It is shown that EPS slightly increases the accuracy of SL prediction with respect to the deterministic forecast (DF) and it is more reliable than it. It is shown that the SL peaks correspond to maxima of uncertainty (as described by the spread of the EPS members) and the values of these maxima increase linearly with the forecast range. Uncertainty on sea level is caused by the uncertainty of the forcing meteorological fields and the quasi linear dynamics of the storm surges plays a minor role on its evolution except it produces a modulation of the uncertainty after the SL peak with period corresponding to that of the main Adriatic seiche. Finally, the error of the EPS mean is correlated with the EPS spread.

The second part of the research focus on the future storm surge scenario, that is estimated using new high resolution data recently produced by EC-Earth, an Earth System Model based on the operational seasonal forecast system of ECMWF. The study considers an ensemble of six 5-year long simulations of the rcp45 scenario (Hazeleger et al. 2006) and compares the 2094-2098 to the 2004-2008 period. EC-Earth sea level pressure and surface wind fields are used as input to HYPSE. The results show that high resolution of wind fields are essential for producing realistic values of storm surge statistic. However, results confirm previous studies in that they show little sensitivity of storm surge levels to climate change.

Il presente lavoro è incentrato sulla previsione dell'acqua alta a Venezia, con particolare riferimento alla marea meteorologica. Un miglioramento di tale previsione si può ottenere affiancando, alla singola previsione deterministica ottenuta utilizzando campi meteo ad alta risoluzione, una previsione probabilistica generata da campi meteo di tipo ensemble. Verrà inoltre studiato l'impatto dei cambiamenti climatici sulla distribuzione statistica dei contributi meteorologici nell'alto Adriatico, facendo uso di nuovi campi meteo ad alta risoluzione per confrontare le statistiche presenti con quelle di fine secolo.

Si presenta un metodo operativo di previsione della marea meteorologica basato sul metodo dell'Ensemble Prediction System (EPS), in modo da aggiungere un'informazione probabilistica alla previsione stessa. Sono stati analizzati dieci eventi significativi del 2009 e del 2010, generando per ciascuno di essi 50 differenti previsioni di marea con il modello idrodinamico HYPSE, utilizzando come input 50 differenti campi meteo ensemble forniti dl centro meteorologico europeo ECMWF. I risultati mostrano un miglioramento della previsione, ottenuta mediando le 50 corse ensemble, rispetto a quella singola ad alta risoluzione, e ad un irrobustimento della stessa tramite l'aggiunta dell'informazione probabilistica. Si evidenzia infine una correlazione tra l'errore e la varianza delle 50 differenti corse.

La seconda parte della ricerca si focalizza sulla simulazione di uno scenario futuro tramite l'utilizzo dello scenario rcp45 ottenuto dal modello EC-Earth. Si analizzano sei serie ensemble lunghe 5 anni riferite al presente (2004-2008) e sei riferite al futuro (2094-2098). Per quanto riguarda le statistiche dei livelli di marea non si riscontrano tuttavia significativi cambiamenti.

Declaration by Candidate

In submitting this thesis for the degree of Doctor of Civil and Environmental Engineering Science of the University of Padova the author acknowledges help from the individuals listed previously and from the authors of sources acknowledged throughout the text, but states that this thesis is entirely his own work.

Table of Contents

List of Tables

List of Figures

Acknowledgements

The author would like to thank his research supervisors, Prof. Luigi D'Alpaos and Prof. Piero Lionello for their sharp thinking, constructive criticism and continued support during the course of this research project. He would also like to thank Ing. Luca Carniello, for introducing him to the world of numerical models working on Venice Lagoon and Northern Adriatic Sea. He is grateful to Dr. Dario Conte for the assistance in solving computer problems and the management of input fields. Finally, he would like to the Venice City Council for the data of hourly SL observation in CNR platform and Venice "Punta Salute" kindly provided.

Contributions to knowledge

The author claims the following contributions to knowledge:

1. The use of ensemble prediction system method to provide the surges in the Northern Adriatic Sea allows to improve the forecast, that becomes more robust.

2. The development of a probabilistic forecast completes the single deterministic forecast, estimating the probability to exceed the interesting values. That is very important to manage the Venice's high water, especially when the mobile gates will be operative.

3. The evaluation of surge uncertainty directly from the meteorological data allows a quickly estimation of the forecast range.

4. The development of EC-Earth model provides a set of high resolution ensemble data, suitable for a present-future comparison of surge statistic, that can vary due to the climate change.

5. The result of this comparison, superimposed with the mean sea level increase, gives a complete statistic distribution of future storm surges in the Northern Adriatic Sea.

Terminology and abbreviations

Some abbreviations recur in the text. Everyone is written in the full version when occur for the first time. However, to avoid possible doubt, is useful to gather them together here in alphabetic order.

CNR platform *Oceanographic tower of ISMAR-CNR situated in the Adriatic sea in front of the Venice lagoon at a distance of 15 km*

DF *Deterministic forecast*

ECMWF *European Centre for Medium Range Forecast*

EMF *Ensemble Mean Forecast*

EPS *Ensemble Prediction System*

HRV *High resolution version*

HYPSE *Hydrostatic Padua Surface Elevation Model*

I.C.P.S.M *Istituzione Centro Previsione e Segnalazione Maree*

IS08 *The statistic model ISPRA-STAT_2008*

ISPRA *Istituto Superiore per la Protezione e la Ricerca Ambientale*

MSLP *Mean sea level pressure*

LRV *Low resolution version*

PS *Punta Salute GAUGE located in Venice city centre*

R *Residual*

SL *Sea level*

SLR *Sea level rise*

1. Introduction

1.1 Background to research

Storm surge is defined as the rise of seawater above mean tidal level. It is a result of surface winds generated by a storm and relatively low surface pressure (AMS Glossary 2nd edit. 2000), with winds having the largest impact on the surge. Storm surge is a major hazard for those coastal areas exposed to tropical and/or extra-tropical cyclones. An example is Hurricane Katrina (2005), that produced a 6-9 m storm surge along coastal Mississippi and Louisiana, which illustrated the devastation that a major storm surge can create in a coastal metropolitan region. (Diliberto et. al 2009). The surge flooded large sections of New Orleans and coastal Mississippi, causing 81 billion of dollars worth of damage (Knabb et al. 2005). Another example of a storm surge catastrophe during the cool season is the severe gale force winds that occurred over the North Sea during the winter of 1953, which resulted in a storm surge that killed over 2,000 people in the Netherlands, United Kingdom, and Belgium. (Diliberto et al. 2009). This led the Netherlands to implement the Delta Plan in 1953 (http://www.deltawerken.com/ /English/10.html), which involved building an intricate series of storm surge barriers throughout this low lying country (Gerritsen 2005, Baxter 2005). In 1970, a typhoon in the Bay of Bengal struck then Bangladesh with a 6 m storm surge that killed 300,000 people (Frank and Husain 1971). Many other example of hurricane storm surge could be explained, but hurricanes are not the only one cause of floods in the coastal area: extra-tropical cyclones can threat a lot of them.

The North Sea storm surge of 31 January 1953 was the worst natural disaster to affect the UK in recent times, causing the loss of 307 lives in East Anglia (Baxter, 2005) and a further 1836 fatalities in the Netherlands (Gerritsen, 2005).

On 4 November 1966 an exceptional storm hit the central and north-eastern part of Italy with very intense precipitation over large areas and strong winds over the Adriatic Sea, east of the Italian peninsula. The storm caused the flood of the greatest historical town of Italy, Venice, inflicted severe damage to the economic and artistic patrimony. In that storm other towns and villages in central and north-eastern Italy, and claimed the lives of more than 100 people (Cavaleri et al. 2010).

To prevent most of the damage due to the surges, an as correct as possible forecast is required. Storm surges are driven by the weather, which is expected to be the dominant source of surge forecast uncertainty: describe and provide it is one of the future development in surge forecast.

The use of ensemble techniques to produce quantitative estimates of uncertainty and risk is well established in the meteorological domain (e.g. Buizza et al., 2005; Bowler et al., 2008; and references therein). Ensemble forecasts of ocean waves have been produced by the European Centre for Medium-Range Weather Forecasts (ECMWF) since June 1998 (Saetra and Bidlot, 2004). For example Mourre et al. (2004) used ensemble techniques to study the impact of bathymetric uncertainty on storm surge forecasts, its implications for assimilation of sea-level data, and the possibility of using such assimilation to correct the bathymetric input. Debernard and Røed (2008) compared climate projections from a storm surge model driven by downscaled output from different global climate models and emissions

scenarios. Diliberto et. al (2009) show that the inclusion of an ensemble using all models available improve the surge forecast. Moreover bias correction applied to the all ensemble helps to reduce the root mean square error and makes the mean error slightly positive over all forecast hours these results have shown the benefits of using a multi-model surge prediction system. Forecasters would benefit if surge predictions from different operational ocean models could be combined, rather than using just one surge model and an atmospheric ensemble. (Diliberto et al. 2009).

Previous studies on storm surge statistic in the Northern Adriatic sea, which have not found clear indications of significant changes (Lionello et al 2003; Lionello et al. 2012), were based on relatively low resolution meteorological fields, which were not able to reproduce correctly the statistic of the most extreme events.

1.2 Justification for the research

Storm surges are major hazards frequently hitting Venice and pose severe problems for the city and its lagoon. An accurate and fully informative prediction of sea level (SL) in the time range from one hour to several days is an essential tool for the management of the city and the delivery of reliable and accurate warnings. Storm surges are driven by the weather, which is expected to be the dominant source of surge forecast uncertainty: describe and provide it is one of the future development in surge forecast. To achieve this goal the ensemble prediction system method should be implemented. A reliable prediction is specifically critical for operating efficiently the flood barriers that the Italian government is presently building, as an important component of the general plan for the safeguard of Venice. The mobile gates

are a system of electromechanical underwater barriers, which will be risen before high storm surge events, stopping the flood from entering the Venice lagoon. The purpose is to prevent SL to rise higher than 110 cm above mean SL in the Venice city centre. The first objective of this research is to include in surge forecast an exceeding probability, due to manage optimally the mobile barriers dams.

Climate change is a threat for coastal towns and cities and those built on islands: sea level rise and storminess are among the major environmental concerns. More extreme sea levels could be also induced by changes in weather extremes, which can imply additional coastal impacts than attributable to sea-level rise alone. However, changes in storm characteristics and intensity are less certain than sea level rise. The statistics of sea level, mean sea level pressure and wind, two variables that are responsible for sea level variations, are analysed with the aim of identifying significant differences between present and future scenario conditions. The second target is to investigate the influence of climate change on storm surge statistics in the Northern Adriatic Sea using a new high resolution climate model simulation, in order to add a new and different contribution to past estimates. It is also important to investigate whether a new set of simulations, using meteorological forcing at higher resolution than earlier studies, produces different conclusions.

1.2.1 Floods threat in Venice

Storm surges damage buildings and coastal defences, affect daily life of venetians and tourism. They represent a threat not only to the artistic and cultural heritage, but also to the economic assets and the environment, and, further, future sea level rise is expected to dramatically change their

frequency (e.g. Lionello, 2012). The two greatest storms in the Northern Adriatic Sea occur on 4 November 1966 (1.94m of observed tide above SL) and on 22 December 1979 (1.66m).

Between 1 and 2 November 1966, a deep tropospheric trough positioned over Spain started intensifying and rotating anticlockwise. By 3 November, the trough deepened very rapidly over Spain, and strong south-easterly and then southerly winds started affecting the mid-troposphere over the Italian peninsula. At the surface on 3 November cyclogenesis started over Spain. The surface cyclone moved over the western Mediterranean and was reinforced by a secondary, small-scale depression coming from North Africa. At the same time, an anticyclone over the Balkans intensified in place. The result was a strong southerly flow over the Adriatic that at the surface, channelled by the bordering orography, led to a strong sirocco wind over the whole basin. As noted in Malguzzi et al. (2006), although the low-pressure centre located over northern Italy was not very deep, the west-to-east pressure gradient, and hence the south-easterly wind over the Adriatic Sea, was very strong: on 4 November, it was further intensified by the advancing cold front from the west, assuming the character of a pre-frontal low-level jet. No report of the surface wind speed over the sea is available, but an unofficial anemometer located at the edge of the Venetian lagoon, very close to the sea coastline, reported sustained winds close to or above 20 m/s from 0800 until 1600 UTC 4 November. As might be expected, no wave measurements were available, but the storm destroyed the final 100–200 metres of the jetties bordering the three inlets connecting the Venice lagoon to the sea. Some of these jetties housed open-sea tide gauges that were obviously wiped out. Tide records exist from the Venice area, inside the

lagoon. However, based on previous experience, these tide gauges had been designed for a maximum level of 1.80 m above the nominal sea level (Cavaleri et al. 2010). The maximum sea level reached during this storm was estimated at +1.94 m from the marks left on the walls by the oil exiting from the flooded tanks and floating on top of the water. Note also that the water in the lagoon was oscillating wildly, reaching different levels at different times and positions. Hence also the 1.94m figure must be considered accurate only to within a few centimetres. Compared to the statistics derived from previous data, recorded since 1872, the 1966 event stands out dramatically, and it was variously judged (Cecconi et al., 1999) to have a return period of 150–300 years. It is interesting to note that two comparable, but not properly quantified, events reported in historical documents happened in 1822 and 1867, when no instrumental measurements were taken (Camuffo, 1993). It seems likely that the latter event triggered the start of official measurements. Another remarkable detail that highlights even further the exceptional character of the 1966 storm is that the flood was entirely due to the storm surge, with actually a negative contribution (-11 cm with respect to the present mean sea level) coming from the astronomical tide. In order to interpret Figure 1 correctly in this respect it is necessary to consider that the actual mean sea level in 1966 was 23 cm higher than the nominal value, established back in 1896 and still in use today (Cavaleri et al. 2010).

The basic meteorological situation of the 1979 storm was similar to the 1966 one, although without the same dramatically strong pressure gradients over the Adriatic area. A deep low-pressure minimum was located west of Italy, over the Tyrrhenian Sea, and contrasted with an anticyclone over eastern Europe. Sustained sirocco winds developed all along the Adriatic

Sea. Due to the reinforced outer ends of the jetty and to the fact that the storm was less extreme than in 1966, in this case no damage was inflicted to the jetties. However, the storm was strong enough to cause severe damage to the superstructures of the oceanographic tower (CNR platform) located in the northern Adriatic Sea 15 km offshore the Venetian coast in a 16-metre depth (Cavaleri et al. 2010).

1.2.2 Problems in surge forecast

This uncertainty can take many forms, including whether a given synoptic system develops in the first place, the track along which it moves, the strength and structure of the associated surface wind and pressure fields, and the timing of these relative to the astronomic tide (Flowerdew et al. 2010). A main source of uncertainty of the forecast carried out with hydrodynamical models is the errors of the input wind fields (Lionello et al. 1998). In fact, in the shallow northern Adriatic the main forcing of the storm surge is the wind stress, which is difficult to predict with sufficient precision by meteorological models, because it presents sharp and irregular meso-scale structures produced by the steep mountains on both sides of the Adriatic sea (e.g. Zecchetto et al. 2001). In practice, the forecasts produced by the hydro-dynamical models can be substantially different from the real evolution of sea level. In principle, atmospheric forcing is not the only source of uncertainty in storm surge forecasts: uncertainty in the surge model formulation, boundary conditions and initial sea state could also be important. For simplicity, these have been neglected in this research, because they can be treat separately, being a source of error that can be superimposed (Flowerdew et al. 2010).

1.2.3 Future flood threats

Future sea level rise will very likely increase the frequency of extreme sea levels. During the 20th century the mean relative sea level in Venice has already increased by 0.3m. Approximately half of it is due to vertical land motion (see Lionello 2012, for a synthesis), with two main contributions: local anthropogenic subsidence, mostly caused by the extraction of groundwater in the past, and long term tectonic vertical motion. While the extraction of ground water has stopped, tectonic motion is expected to continue, though eventually not at a regular pace. Further, sea level is expected to rise in future, though its regional evolution is uncertain and cannot be easily related to global sea level rise, because of likely future halosteric contraction and difficulty to model future mass exchanges between Mediterranean Sea and Atlantic ocean (Lionello 2012, Scarascia and Lionello, submitted).

1.3 The tide in Venice

On the short time scale (hours to few days) the sea level variations in the northern Adriatic are caused by three factors: astronomical tide, storm surge and seiches (free oscillations of water level).

1.3.1 Astronomical tide

Astronomical tide is caused by the varying gravitational attraction of the Sun and the Moon. It consists in the superposition of sinusoidal oscillations (in the Adriatic Sea about eight components are needed for reaching a good accuracy) and is predicted with very high precision on the basis of harmonic analysis of sufficiently long time series.

1.3.2 Meteorological contribution

Meteorological contribution (storm surge) is caused by meteorological factors (surface wind and mean sea level pressure, MSLP), which alter the regular oscillation due to astronomical tide and can produce the positive anomalies that cause the flooding of Venice (the well-known “Aqua Alta”). The Adriatic Sea is long (800km), relatively narrow (generally less than 200km wide), with very shallow water in its northern part in front of the Venetian coast. Its morphology favours the action of Sirocco, a strong wind, which blowing north-westwards along the axis of the basin, accumulates water at the closed end of the Adriatic and whose effect is reinforced by the action of the MSLP gradient (inverse barometric effect). Nonlinear effects associated with interaction between surge and astronomical tide in shallow waters are negligible in the Adriatic Sea (Lionello et al. 2006) so that tides and storm surge can be computed independently and superimposed without introducing a relevant error. Therefore, the crucial problem for the prediction of water level in the northern Adriatic is the correct computation of the storm surge component..

1.3.3 Seiches

Seiches are longitudinal and transverse free oscillations (their fundamental periods are about 11 and 22 hours) that are triggered by an initial storm surge event and whose amplitude is successively decreased by dissipation. In fact, the Adriatic basin, because of its geometry, behaves for sea level as a resonant cavity for sound waves, with seiches being the analogue of normal oscillation modes (e.g. Lionello et al. 2005). In this manuscript the superposition of storm surge and seiches (which is the SL

without astronomical tide) is synthetically called meteorological contribution.

1.3.4 Tide forecast

Because of the big damage that was produced by the large flood in 1966 and the problems that recurrent floods pose to Venice, a tide forecast centre has been established in 1980 (I.C.P.S.M. - Istituzione Centro Previsioni e Segnalazioni Maree), which operates a set of models for sea level prediction. The demand for a precise forecast over a long time range has been recently increased by the construction of mobile gates, which, by closing the inlets of the Venice lagoon, will prevent the flooding of the city.

The model initially used for operational forecasting of SL in Venice is a linear statistical autoregressive model (Tomasin 1972), which is calibrated using observed sea level time series (the tide gauge station "Punta Salute" is now operating for over a century in the Venice city centre). This model predicts the water level in the lagoon using observed local sea level and MSLP at stations along the Adriatic Sea and its evolution (called BIGSUMDP) is still nowadays in use with very good results. However, this autoregressive model looses reliability when prediction over a time range longer than one day is required (Canestrelli 2000). I.C.P.S.M. has, therefore, adopted hydro-dynamical models, which are directly based on the "shallow water" equations and compute the evolution of current and sea level from a sequence of MSLP and surface wind fields. These models allow a reliable forecast over a longer time range and their accuracy is mostly determined by their spatial resolution and by the quality of the forcing meteorological fields. The two models that are presently used are SHYFEM (Shallow Water Hydrodynamic Finite Element Model, Umgiesser et al., 2004), based on the

finite element method, and HYPSEAM (HYdrostatic Padua Sea Elevation and Adjoint Model, Lionello et al., 2006), which includes a data assimilation procedure based on the adjoint method.

The forecasts produced by the hydro-dynamical models can be substantially different from the real evolution of sea level. While, in general, hydro-dynamical models are more accurate for hourly sea level, models based on the statistical autoregressive approach produce better results if only high storm surges are considered. The hydrodynamic model SHYFEM with a post-processing method, based on the use of neural networks to improve the surge prediction, has been developed and validated. It reduces the standard deviation of about 20%. (Bajo et Umgiesser, 2010).

Model	***24h***	***48h***	***72h***
Events > 100cm			
BIGSUMDP	-3.0 ± 17.6	-6.3 ± 20.7	-7.2 ± 27.0
SHYFEM v3	-8.0 ± 22.2	-12.3 ± 26.5	-18.1 ± 31.6
Hourly sea level			
BIGSUMDP	-0.8 ± 11.9	-1.6 ± 14.9	-2.2 ± 16.7
SHYFEM v3	0.3 ± 12.4	-0.2 ± 15.1	-0.8 ± 17.8

Table I Mean error ± twice its standard deviation for the operational forecast produced by the auto regressive statistical model BIGSUMDP and the hydrodynamic model SHYFEM at ICPSM. The forecast range 24, 48, 72hours are considered. The statistics refer to the period 1st August 2008 – 31st July 2011. The statistics on 97 events higher than 100cm and on hourly data are computed separately (source of data: http://www.comune.venezia.it/flex/cm/pages/ /ServeBLOB.php/L/IT/IDPagina/38974).

1.3.5 Subsidence and eustatism scenarios

For most coastal zones, sea level rise is the most dangerous aspect of climate change. In the Adriatic Sea it would affect many small islands along the Croatian coast and the whole low coast of the Po and Venetian-Friuli plains, including the unique environment of the Venetian lagoon and the city itself. Besides producing direct effects (loss of economically valuable areas, salt intrusion in aquifers, increased coastal erosion, etc.), sea level rise might change the characteristics of free (seiches) and forced (tides and storm surges) oscillations of the Adriatic Sea. The implications of sea level rise (SLR) should be accounted for in planning coastal protection and future harbour management.

Present estimates of SLR and uncertainties are summarized in the 3rd report of the Intergovernmental Panel on Climate Change (Houghton et al. 2001). During the 20th century SLR was in the range 1.0 to 2.0 mm yr−1. Projected SLR, accounting for several possible scenarios, ranges from 0.09 to 0.88m by 2100. Projections further on in time have, obviously, an even larger uncertainty. However, SLR will continue, even if green house gases concentrations stabilise. Thermal expansion alone could contribute 1 to 4 m for CO2 levels of twice and 4 times the pre-industrial period, respectively. The speed of such growth would depend on the penetration of the temperature increase into the ocean interior. A reasonable estimate is a SLR between 0.5 and 1 m in 500 yr. The melting of polar ice sheets would potentially add a extremely large contribution to SLR. The Greenland icesheet is the most vulnerable, and for a warming between 5.5°C (consistent with mid-range green houses gasses) stabilisation scenarios and 8°C, it could contribute between 3 and 6 m to SLR in 1000 yr (Houghton et al. 2001). The

sea level of the Mediterranean is not always immediately related to the global one. It increased consistently with the mean global value through the 1960s (Church et al. 2001), but it subsequently dropped by 2 to 3 cm until the beginning of the 1990s (Tsimplis & Baker 2000). During the last decade of the 20th century, Mediterranean sea level increased 10 times faster than the global ocean scale (Fenoglio-Marc 2002). Reasons for this behavior are not well known, but it is not conceivable in the long term that the Mediterranean Sea level can be uncoupled from large changes of the global one. In brief, although there has been a large sea level rise during relatively recent history (sea level was 120 m below present level during the last glacial maximum about 20 000 yr ago) the largest SLR expected in one century is below 1 m, and a SLR of several meters is possible only on multi-centennial time scales. All these estimates are subjected to very large uncertainties.

1.4 Climate change

Climate refers to the average weather given by the statistics of temperature, humidity, atmospheric pressure, wind, precipitation, atmospheric particle count and other meteorological elemental measurements in a given region over long periods (usually 30 years).

Climate varies from place to place, depending on latitude, altitude, terrain, distance to the sea, vegetation, presence or absence of mountains or other geographical factors. It varies also in time; from season to season, year to year, decade to decade or on much longer time-scales, such as the Ice Ages. A region's climate is generated by the climate system, which is an interactive system consisting of five major components: atmosphere,

hydrosphere, cryosphere, land surface, and biosphere. They are forced by external forcing, such as the Sun, and by the effects of human activities. The climate system is extremely complex, due to the interactions among the components; indeed many physical, chemical and biological interaction processes occur between them, on a wide range of space and time scales.

Although these components are very different in their composition, physical and chemical properties, structure and behaviour, they are all linked by fluxes of mass, heat and momentum: all subsystems are open and interrelated. Their changes, whether natural or anthropogenic, or changes in the external forcing, may result in climate variations.

Climate change is the long-term shift in weather patterns in a specific region or globally that can be identified, using statistical tests, by changes in the mean and/or the variability of its properties and that persists for an extended period, typically decades or longer. Unlike global warming, which refers to just one aspect of climate change, a rise in the surface temperature of the earth, climate change refers to changes in the overall weather patterns of a region, including precipitation, temperatures, cloud cover, and so on. Climate change may be due to natural internal processes or external forcing, in which case it may be partly predictable, particularly on the larger, continental and global, spatial scales. Another cause is the persistent anthropogenic change in the composition of the atmosphere or in land use, however because human activities do result in external forcing, it is believe that the large scale aspects of human-induced climate change are also partly predictable.

Unfortunately the ability to actually do so is limited because it is not possible to accurately predict the most important characteristics of future

human activity. In practice scenarios of human behaviour are constructed, and climate projections on the basis of such scenarios are made. This is done by seeing climate models, large computer programs solve the governing equations of atmospheric and ocean fields and the physical processes that occur. One climate model is EC-Earth (Hazeleger et al. 2006), which is used in this study.

1.4.1 Natural and human factors of climate change

There are a number of natural factors responsible for climate change. Some of the more prominent ones are radiative forcing, volcanoes, ocean currents, orbital parameters and continental drift.

Radiative forcing: a change in either the solar and infrared radiation changes the average net radiation from zero, the equilibrium climate state value.

Volcanoes: when a volcano erupts it throws out large volumes of sulphur dioxide (SO2), water vapour, dust, and ash into the atmosphere. These large volumes of gases and ash can influence climatic patterns for one or two years, by reflecting solar radiations.

Ocean currents: the ocean is a major driver of global climate. It redistributes large amounts of heat around the planet by global ocean currents and through regional scale upwelling and downwelling. Oceans and global temperature change are connected as warm waters create warmer temperatures and vice versa.

Orbital parameters: changes in the earth tilt, eccentricity and obliquity can affect the severity of the seasons.

Continental drift: the continents were formed when the landmass began gradually drifting apart, millions of years back. This drift also had an impact on the climate because it changed the physical features of the landmass, their position and the position of water bodies. The separation of the landmasses changed the flow of ocean currents and winds, which affected the climate. This drift of the continents continues even today, but is very slow.

For three centuries human activities have an impact on regional and global climate. The most important ways are the increasing of aerosols and greenhouse gases and changes of land use.

The enhanced greenhouse effect: fossil fuels such as oil, coal and natural gas supply most of the energy needed to run vehicles, generate electricity for industries, households, etc. All this has contributed to a rise in greenhouse gases in the atmosphere, like water vapour and carbon dioxide. Changes in land use pattern, deforestation, land clearing, agriculture, and other activities have all led to a rise in the emission of carbon dioxide. Methane and nitrous oxide are the others important greenhouses gas in the atmosphere. Greenhouses gasses reduce the rate at which the Earth's surface loses infrared radiation to outer space. Because one way to increase the temperature of anything is to reduce its rate of energy loss to its surroundings, this makes the Earth's surface and lower atmosphere warmer than they would otherwise be.

Land use change: the Industrial Revolution in the 19th century saw the large-scale use of fossil fuels for industrial activities. These industries created jobs and over the years, people moved from rural areas to the cities. This trend is continuing even today. More and more land that was covered with vegetation has been cleared to make way for agriculture and houses.

Land use change may contribute significantly to changing the local, regional or even global climate and moreover has an important impact on the carbon cycle.

The effect of aerosols: aerosols are a colloid suspensions of fine solid particles or liquid droplets in a gas. They are involved in the radiative balance, that is altered due to the increasing amount of aerosols. However the effect of their concentration change is very complex and not yet well known.

1.4.2 Global effects

Additional data from new studies of current and paleo-climates, improved analysis of data sets, more rigorous evaluation of their quality, and comparisons among data from different sources have led to greater understanding of climate change, occurring as a result of both internal variability within the climate system and external factors (both natural and anthropogenic).

However current and future climate change is caused by human activities that have resulted in an increased concentration of greenhouse gases in our atmosphere, including carbon dioxide, water vapor, methane, ozone, and nitrous oxide. Climate change on this scale will produce results such as the following:

* Increased surface temperatures

* Rises in sea levels

* Retreat of glaciers and melting of sea ice

* Changes in precipitation

* Increases in intensity of extreme weather events

* Longer, more severe droughts

* Expansion of subtropical deserts

* Species endangerment and extinction and loss of biodiversity

* Melting of permafrost

* Drops in agricultural yields

* Spread of vector-borne diseases because of increased range of insects

* Acidification of oceans creating drops in fishing yields and death of coral reefs.

2. Models and data

In this research storm surge events in Northern Adriatic Sea are simulated, run both the shallow water hydrodynamic model HYPSE and the statistic model IS08. They uses as input meteorological data fields, MSLP, U and V wind components, provided by ECMWF.

2.1 Meteorological data

For the application of EPS method to surge forecast the storm surge events are simulated producing for each of them an ensemble of 50 simulations, using as input a set of 50 wind and pressure fields provided by ECMWF.

For the study of future surge scenario new high resolution data recently produced by EC-Earth, an Earth System Model based on the operational seasonal forecast system of ECMWF are used. The study considers an ensemble of six 5-year long simulations of the rcp45 scenario and compares the 2094-2098 to the 2004-2008 period.

2.1.1 ECMWF ensemble data set

Wind and MSLP fields are provided by ECMWF. The centre supplies 3-hourly MSLP and surface wind fields of both EPS and high resolution deterministic forecast. The ECMWF EPS fields represent uncertainty in the initial conditions by a set of 50 forecasts starting from slightly different initial conditions, whose differences have the same order of magnitude of the uncertainties on the initial state of the atmosphere. Each forecast is also based on a model which is close, but not identical, to the best estimate of the model equations, thus representing also the influence of model uncertainties

on forecast error. The perturbations are not generated at random (as would be the case with a pure Monte Carlo technique), instead, they are a combination of 25 modes that have the largest impact on the short range forecast for the Northern Hemisphere (ECMWF Technical Memorandum No 188, August 1992).

2.1.2 EC-Earth

Despite their different purposes, climate and weather forecasting are obviously based on the same physical principles. This has been recognized with the introduction of the concept of "seamless prediction", which intends to address the predictability of the climate (in its broadest sense) within one common framework. Therefore EC-Earth was developed (Hazeleger et al. 2006), an Earth System Model based on the operational seasonal forecast system of the European Centre for Medium-Range Weather Forecasts (ECMWF). It is intended to investigate Earth system feedbacks, study interannual and multi-decadal climate fluctuations and predictability, and to be an advanced modelling tool for computing climate scenarios.

The development of EC-Earth within the EC-Earth consortium started with ECMWF's Integrated Forecast System (IFS) as a well-tested atmospheric module, with different components being added over time. In the current version (V2.3) of EC-Earth an interactive atmosphere–ocean-sea ice coupling is applied across the entire globe, including the polar regions, using different sea ice and land modules.

In a present day control run the large-scale characteristics of the atmosphere, such as the distributions of sea level pressure, temperature and humidity distributions are well simulated, as compared to observations,

reanalysis data and other coupled atmosphere–ocean-sea ice models. When forced by increasing concentrations of greenhouses gases to simulate the future climate, EC-Earth shows similar responses as found in earlier model studies: the tropospheric warming with a maximum in the higher tropical troposphere, stratospheric cooling, polar amplification of the climate change signal, changes of the hydrological cycle in line with most of IPCC models.

EC Earth has been developed with two kind of resolution: one low resolution version (LRV), with a grid step of 1.125 degrees, and one high resolution version (HRV), with 0.25 degrees of grid step. Besides the resolution, the two versions differ also by the kind of coupling; LRV is a fully coupled climate model while HRV is atmosphere only, with SST (sea surface temperature) prescribed from the LRV. To study the possible changes in Northern Adriatic Sea storminess, EC-Earth data fields are chosen.

2.2 Hydrodynamical model HYPSE

The simulations carried out in this study are based on HYPSE (Lionello et al. 2005), which is a standard single-layer nonlinear shallow water model, whose equations are derived from the vertical average of the momentum equation, assuming a constant velocity profile. It adopts an orthogonal C-grid and uses the leap-frog time integration scheme with the Asselin filter to prevent time splitting. The model computes the total transport U = (U, V) and the sea surface elevation, solving the vertically integrated momentum equations:

$$\frac{\delta U}{\delta t} = -g(H+\eta)\cdot\frac{\delta}{\delta x}\left(\eta + \frac{p_a}{\rho_w g}\right) + fV + \frac{\tau_{xb} - \tau_{zb}}{\rho_w} - \nabla\int_{-H}^{\eta}(\Gamma(u) + \overline{uv})dz \qquad (1)$$

$$\frac{\delta V}{\delta t} = -g(H+\eta)\cdot\frac{\delta}{\delta y}\left(\eta + \frac{p_a}{\rho_w g}\right) - fU + \frac{\tau_{yb} - \tau_{zb}}{\rho_w} - \nabla\int_{-H}^{\eta}(\Gamma(v) + \overline{vv})dz \qquad (2)$$

$$\frac{\delta \eta}{\delta t} = -\left(\frac{\delta U}{\delta x} + \frac{\delta V}{\delta y}\right) \qquad (3)$$

It includes meteorological contribution (sea level pressure p_a and wind stress) and a quadratic bottom stress

$$\vec{\tau_b} = -\rho_w b_f \vec{u}|\vec{u}| \qquad (4)$$

where

$$b_f = 5\cdot 10^{-3} \qquad c_s = 0.4 \qquad (5)$$

and a Smagorinsky horizontal diffusivity with coefficient:

$$A = c_s \Delta x \Delta y\left[\left(\frac{\delta u}{\delta x}\right)^2 + \left(\frac{\delta v}{\delta y}\right)^2 + \frac{1}{2}\left(\frac{\delta v}{\delta x} + \frac{\delta u}{\delta y}\right)^2\right] \qquad (6)$$

where u,v are the depth-averaged current velocity components, Δx and Δy are the grid steps, b_f and c_s are two coefficients, whose value has been chosen to optimize the model results.

During the forcing of the model due to meteorological fields, the stress is parametrized in the following way.

$$\vec{\tau_w} = \rho_a C_D U_{10}\vec{U}_{10} \qquad (7)$$

$$C_D = A + BU_{10} \qquad (8)$$

$$A = 8 \cdot 10^{-4}; B = 8.4 \cdot 10^{-5}\ s/m \qquad if \quad U_{10} > 4.8 s/m$$

$$A = 1.2 \cdot 10^{-3}; B = 0\, s/m \qquad if \quad U_{10} < 4.8 s/m \tag{9}$$

where U_{10} is the 10m wind speed; A and B are two coefficients depending on U_{10}. Metric factors enter the expression actually used in the model, considering the earth's curvature.

The model's reliability depends on resolution and on the grid used for its implementation. It covers only the Adriatic sea, with null elevation as boundary condition in the south-eastern area (Otranto channel). This excludes the effects of storms that occur outside, in order to understand the change only inside the Adriatic sea, the aim of this work.

The grid used in this study has been selected in order to optimize the results in the North Adriatic with a higher resolution in this part than in the rest of the basin. In this implementation the model uses a rectangular mesh grid of variable size, which has the highest resolution in the northern part of the basin, where the minimum step is 0.03 degrees. Starting from that point, the grid step increases with a logarithmic increment (which uses a 1.01 factor) in both latitude and longitude. Pratically, its resolution varies in the range from 3.3 to 7km, covering the whole Adriatic with Nx=133 and Ny=146 points in longitude and latitude, respectively. Model details and validation are described in Lionello et al. 2005 and 2006.

2.3 Statistic model

The model ISPRA-STAT_2008 (IS08), developed and operative in ISPRA, (http://gnoo.bo.ingv.it/convegno_gnoo_2010) use a statistical approach where the physical process that generates the phenomenon are not considered. It goes to seek a linear autoregressive schema, which relating the surge through a series of characteristic coefficients provided with the values for the various predictors.

The model uses 24 hours of observed parameters and 72 hours (duration of forecast) of provided parameters. Observed parameters are tide level on PS, wind speed on CNR platform, mean sea level pressure on Genoa, P. Torres, Bari and Venice. Provided parameters, obtained from the same ECMWF fields used in HYPSE, are the tri-times values of atmospheric pressure on Genoa, P. Torres, Bari and Venice and wind on CNR platform. The model employs wind only if it blows from first or second quadrant (Bora and Sirocco).

The reliability tests performed on the estimates provided by IS08 show very good results. For example, in the prediction to 48 hours at Punta Salute, the standard deviation on the errors has been judged 7 cm in the calibration phase, and was equal to 8 cm, in the operational phase. The accuracy of the prediction degrades slightly in the case of events of high water (isolating events above 0.8 m, the standard deviation grows up to 0.12 m), for which the model shows, in general, a tendency to underestimate of the maximum level.

3. Probabilistic forecast

3.1 Introduction

Due to the sensitivity of the surge prediction to the wind fields this error in input spoils the sea level forecast, which error could be significant: a single-deterministic tide forecast could be far from the observed tide, is also impossible with that kind of forecast to know its uncertainty that will be indispensable in order to manage the decision of inlets gates closure. Reaching this target requires operating the barriers sufficiently in advance before the peak of the event for ensuring SL not to cross this limit even for long surges (up to 36 hours), when the leakage of the barriers cannot be neglected. Though the barriers need only 30 minutes for closing the lagoon inlets, three more hours are needed to stop the ship traffic, and up to five hours are required to compensate for the leakage of the barriers and keep SL below the threshold (Eprim et al. 2005). Clearly an accurate and fully informative forecast is important for achieving this goal.

To realize this, it needs to act on the kind of meteorological fields used in surge-forecast, using for each event more meteorological forecasts in order to use together with the single high resolution forecast, to determine its uncertainty.

3.1.1 Ensemble prediction system

The ensemble prediction system (EPS, Molteni et al., 1996) is since 1992 operational at ECMWF. It is a consolidated tool that provides a probabilistic weather prediction. The conceptual background of EPS is chaos theory, which describes the behaviour of dynamical systems that are highly sensitive

to the initial condition (the so-called chaotic systems, such as the atmosphere). The behaviour of chaotic systems is, in fact, unpredictable, even though these systems are governed by deterministic equations and their future evolution can be predicted exactly from the initial condition. In fact, despite enormous advances in the observational network, it will always be impossible to describe the state of the atmosphere without any uncertainty. As very small initial condition errors can amplify rapidly in time, the result of weather forecasts will deviate from the actual evolution of weather (Lorenz, 1965) in an unpredictable way. The EPS consists of a set of different forecasts based on a set of different initial conditions, which are designed to represent uncertainties inherent in the operational analysis by introducing those perturbations that grow most rapidly in time. The problem is formalised mathematically using the singular vector technique (Buizza and Palmer, 1995). EPS estimates the probability distribution function of forecast states and provides a practical tool for estimating how this initial error affects the forecast.

3.1.2 Application of EPS in surge forecast

In this research we use the ECMWF EPS for producing a corresponding EPS of sea level in the Adriatic Sea. The basic idea is to use each member of the ECMWF EPS for obtaining a corresponding forecast of SL and use this set of SL for a probabilistic prediction. Multi-model storm surge ensemble prediction has been performed for New York and the North Sea by Diliberto et al 2011 and Siek et al 2011, respectively. Both studies found that the prediction accuracy of multi-mode ensemble is considerably improved in comparison to the one achieved by single models. However, the study, follows the approach of Flowerdew et al 2009, 2010, 2012, who

implemented EPS for storm surges in the North Sea showed that the ensemble spread is indeed a reliable indicator of the uncertainty associated with large surge events and obtained a skilled probabilistic forecast which led to the operational implementation of the EPS system. This study is meant to investigate the effectiveness and utility of the EPS approach in a different situation, where the wind fields are strongly affected by local features (e.g. Zecchetto et al. 2001) the SL dynamics has a lower range than in the North Sea and includes large seiches. Finally, the city of Venice and its lagoon represent a situation where a probabilistic prediction can provide very important information for the management of coastal defences.

3.2 Method of work

In this study ten events, which occurred in 2009 and 2010 are studied. For each event 51 different SL forecasts are produced by HYPSE: 50 forecasts are based on the EPS fields, plus one based on the ECMWF high resolution meteorological forecast (deterministic forecast). This single deterministic forecast is presently used for sea level forecast in Venice together with the forecasts produced by SHYFEM and BIGSUMDP. The HYPSE model is exactly the same in all 51 forecasts, which for sea level and current adopt the same initial condition, which is obtained with a six days simulations (analysis) during which HYPSE is forced by the ECMWF analysis. In other words, each of the 51 simulations is split into two parts: a six day analysis (identical for all 51 simulations) and a six day forecast, each presenting a different sea level evolution because of the 51 different forcing.

Any surge event chosen follows long periods of meteorological quiet, this solution allows to use an only 6 day long warm up period. It is enough

for the Adriatic Sea surge forecast, longer warm up periods don't improve significantly (below 1%) it. The 50 member SL ensemble is meant to provide information on sea level uncertainty (probabilistic prediction) and the deterministic forecast (DF) is meant to be the best available individual forecast.

3.2.1 Work done

The analysis of the results is based on comparing the model hourly data with the hourly observed SL at CNR platform, located 15km offshore. This tide gauge is preferred to the historical gauge in the Venice city centre because it is not affected by the internal hydrodynamics of the lagoon, which introduces a small delay and slightly modifies the SL signal. For each event 5 prediction ranges have been considered, corresponding to forecast launched at 00 UTC, approximately 24, 48, 72, 96 and 120 hours before the observed peak of sea level. Therefore the study is based on 10x5x51 simulations of HYPSE. Each simulation reproduces the meteorological contribution and the following seiches, which have no appreciable nonlinear interaction with the astronomical tide, which has to be added for obtaining the actual SL, but is not a source of uncertainty to be considered in this study.

Figure 1 Hypse domain with location of CNR platform gauge (black bullet).

3.2.2 Events simulated

The 10 events selected in this study are listed in table 1 and belong to the period 2009-2010 during which the ECMWF EPS system (kind of equations and resolution) was not modified. The list includes events sufficiently intense to be practically relevant (in all events a non negligible fraction of Venice was flooded) and with no major storm surge in the previous two weeks, so that the initial sea level state was not perturbed by pre-existing seiches (this is useful to reduce the warm up run period and the errors related to the initial conditions). Table 2 shows for each event date, time, observed maximum sea level in the city centre, percent of city flooded and maximum surge at the CNR platform.

Event n.	Data of peak	Hour of peak	Observed SL (P.TA SALUTE)	% flooding	Meteo contribution (PLATFORM-CNR)
1	03.02.09	03:15	1.19 m	27 %	0.71 m
2	05.03.09	04:15	0.98 m	4 %	0.60 m
3	29.03.09	22.25	1.16 m	20 %	0.81 m
4	27.04.09	23.25	1.17 m	23 %	0.52 m
5	30.11.09	09.00	1.31 m	48 %	0.58 m
6	06.02.10	01.55	0.84 m	1 %	0.45 m
7	20.02.10	00.50	1.24 m	36 %	0.82 m
8	09.11.10	11.45	1.06 m	9 %	0.56 m
9	22.11.10	00.10	1.22 m	32 %	0.73 m
10	24.12.10	01.00	1.44 m	64 %	0.72 m

Table II Events analyzed in this study: date, time, observed maximum sea level in the city centre, percent of city flooded and maximum surge at the CNR platform, where data have been analyzed.

3.3 Hypse results

Fig.2 shows an example of EPS result: for event 7 the 50 simulations of the EPS launched approximately 3 days before the maximum sea level (thin coloured lines), the DF (thick green line) and the observations (line with black dots). The DF and whole set of EPS forecasts start from the same initial conditions, because of the common 6day analysis, whose last day is shown by the black line. The figure clearly shows the divergence of the

forecasts with time and its large increase during the actual storm surge event in the second day of the simulations.

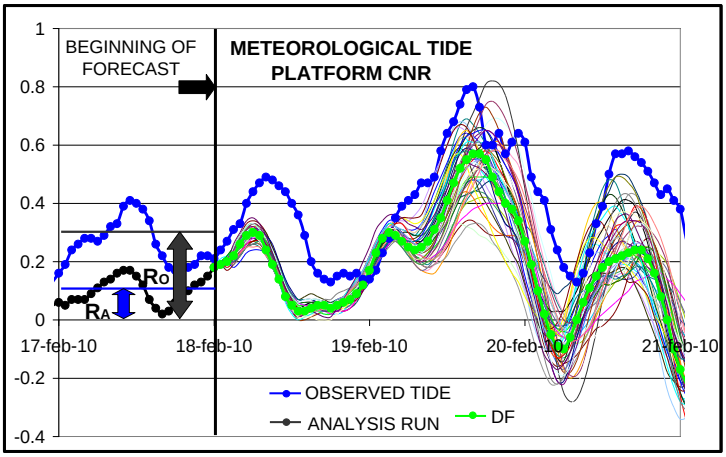

Figure 2 SL forecasts that were launched approximately 48 hours before the peak of event 7. The figure shows the observed SL at the CNR platform (blue line with dots) after subtracting the astronomical tide, the EPS simulations (thin coloured lines), the DF (green line with dots). The last day of the previous analysis is also shown (black line with dots). The figure reports also R_A e $R_{O,}$ the background values which are meant to account for the mean SL of the Adriatic at the onset of the event, for observation and forecast respectively. These values are described in cap. 3.4.

3.4 Improvements

3.4.1 Preliminary normalization of the time series

The set of 10 events considered in this study is rather small for statistical analysis and, further, the events have rather different amplitudes. Therefore, it has been decided to normalize the time series H_i , where i denotes the time step, in such a way to reduce them to a dimensionless index H_{ni}, which facilitates their comparison:

$$Hn_i = \frac{(H_i - R)}{(H_{Max} - R)} \tag{10}$$

Here H_{max} is the observed SL maximum during each event, H_i the i-th hourly value, R a background value which is meant to account for the mean SL of the Adriatic at the onset the event. R is associated with hysteresis effects and changes of Adriatic total water mass. The comparison with observations needs to disregard these two factors, since the physics of the barotropic model cannot account for steric effects (changes of density due to changes of temperature and salinity) and its domain (which is limited to the Adriatic Sea) cannot account for fluxes of mass across the Otranto Strait connecting the basin to the rest of the Mediterranean Sea. In general all the physical involved mechanisms (heat and evaporation fluxes, persistent MSLP gradients at a scale larger than that of the Adriatic Sea) act on a time scale much larger that the storm surge and can offset for a long time the level of the whole Adriatic. In this study R is estimated as the value at the beginning of the forecast of the linear interpolation to the hourly data of the last day of the analysis (see fig.2 and 3). For each event a value of R is computed separately for observations (R_O) and for the forecast (R_A), as it is shown in Fig.3. H_{max} is the maximum observed storm surge level and it is used for the 51 model simulation and the observed time series. Fig.3 shows the effect of the normalization procedure for event n.10. All observed time series reach a peak value equal to 1 (dimensionless), while the forecasts can be larger/smaller than 1 depending they overestimate/underestimate the observed SL peak. Fig.3 shows also the values of R_O, R_A and H_{max}. The following comparisons of the work consider almost always normalized time series.

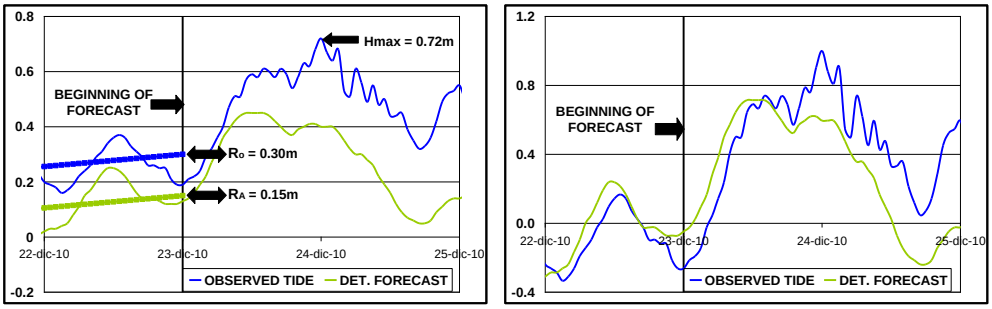

Figure 3 Event n10 on 24.12.2010, 24hour forecast. Left panel: original SL values (in cm) showing the observed time series (blue line) and the DF (green line). The value of R_O, R_A and of H_{max} are 0.30 m, 0.15 m and 0.72 m respectively. The right panel shows the observed time series and DF after the application of the normalization procedure in eq. (10).

3.4.2 Accuracy of deterministic and EPS mean forecast

Table 3 shows the SL peak values of the forecasts launched approximately 24 hours before the peak. It shows for the 10 events the (normalized) DF, the EMF (the mean of the 50 EPS simulations denoted as EMF, Ensemble Mean Forecast), the maximum and minimum SL peak of the EPS simulations, their spread, the error of the deterministic forecast and of the EMF. For the DF and EPS simulations the peak SL is actually the maximum value within a 7-hour time window centered at the time of the observed peak. However, such value, represents in 97% of runs the actual SL maximum of the simulation. The value 1 would characterize a perfect forecast of the peak SL. The table shows that the average behaviour of the EMF is slightly more accurate than that of the deterministic prediction and that (except for event 3) the EPS range always include the observed value. Fig. 4 shows the mean (average of the set of 10 events) results for 12hours, 48hours and 72houts forecast. The quality of the DF and of the EMF is very similar. Both systematically underestimate the observed level (mean values are lower than 1) and the mean absolute error of the SLpeak does not change

with the forecast time range. Note that, because of the 7-hour time window used for identifying the peak, this outcomes does not account for errors in the time of SL peak. Fig 4 shows that the range on the ensemble (the difference between the member predicting the highest and the lowest peak) increases with the forecast range.

	1	**2**	**3**	**4**	**5**	**6**	**7**	**8**	**9**	**10**	**MEAN**
DF	0.30	0.86	0.84	1.48	0.78	0.93	0.73	1.21	0.27	0.83	0.73
EMF	0.45	0.85	0.69	1.09	0.87	0.95	0.83	1.19	0.49	0.61	0.76
EPS max	1.07	1.33	0.79	1.52	1.00	1.36	1.17	1.87	1.01	1.05	1.07
EPS min	0.10	0.63	0.49	0.56	0.74	0.71	0.58	0.82	0.19	0.32	0.51
RANGE	0.97	0.70	0.30	0.96	0.26	0.64	0.60	1.05	0.82	0.53	0.68
Abs. error DF	0.70	0.14	0.16	0.48	0.22	0.07	0.27	0.21	0.73	0.17	0.32
Abs. error EMF	0.55	0.15	0.31	0.09	0.13	0.05	0.17	0.19	0.51	0.39	0.25

Table III 24h forecast for the 10 events. First and second row show the peak SL of the DF and of the EMF, respectively. The third (fourth) row the maximum (minimum) of the EPS, the fifth row the difference (range) between maximum and minimum. The last two rows show the absolute error of DF and EMF. The last column on the right shows for all these variables the mean of all 10 events. All the values are normalized. Peaks are considered inside a +- 3 hour window around the observed peak. For 48 and 72 the results are very similar and are summarized in Fig.4.

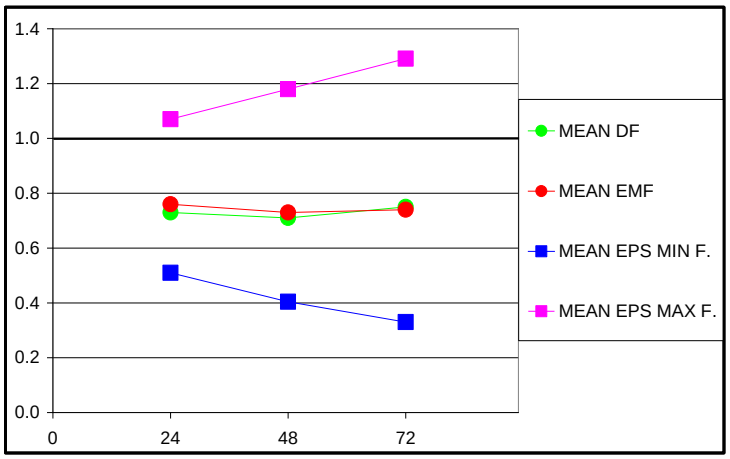

Figure 4 Mean (average values over the 10 events) results of the DF (green dots), of the EMF (red dots), of the highest (pink dots) and lowest (blue dots) members of the EPS.

Figure 5 shows the arithmetic mean of the normalized time series for the set of 10 events: observed surge is compared with the mean of DF and EMF for a 24 hours forecast. Besides the normalization procedure, time series have been shifted in time so that 0 corresponds to the observed peak of the surge. The figure is meant to represent the average "idealized" evolution of a typical surge in the Northern Adriatic and of its prediction. Individual events may deviate substantially from this idealized average evolution (e.g fig.3). It is clear from fig 5 that the characteristic time scale for the evolution of the surge is about half day and the initial peak is followed by the seiches oscillating with a time period of about 22 hours. It is evident that EMF and DF are in general very similar. They both tend to underestimate the actual surge and to slightly anticipate it. On this respect there is no advantage using the EMF with respect to the DF. However, the forecast based on the EMF appear more robust as it is unlikely to be completely wrong. This is shown in Fig.6, where the time evolution of the mean and the maximum error is displayed for the 24hour forecast. Mean and maximum error increase with time for both DF and EMF, but the EMF, although the different resolution, is

systematically lower, because it comes from a 50-runs mean. Further the maximum error of the EMF has a smoother time evolution and is much lower most of the times that the maximum error of the deterministic prediction. Results for longer forecast range (48 and 72 hours) are similar as the EMF has consistently lower errors than the deterministic forecast.

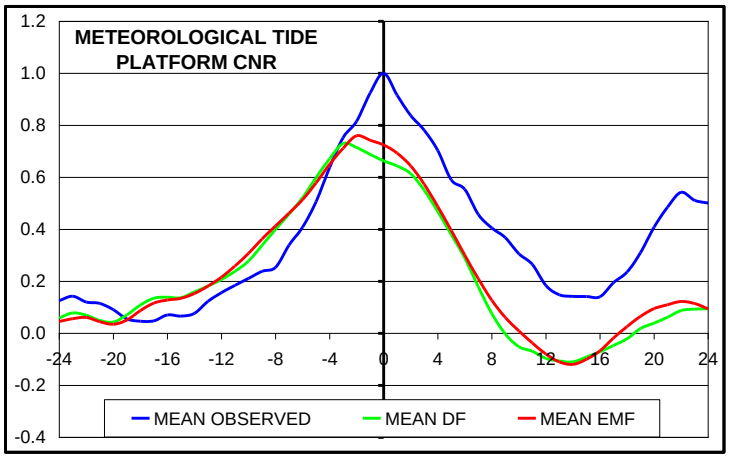

Figure 5 Mean evolution of the normalized time series of the ten events listed in table I considering the 24h forecast and the time range from -24 to +24 hours respect to the observed peak. The observed SL at the CNR platform (blue line), the EMF simulations (red line) and the DF (green line) are shown.

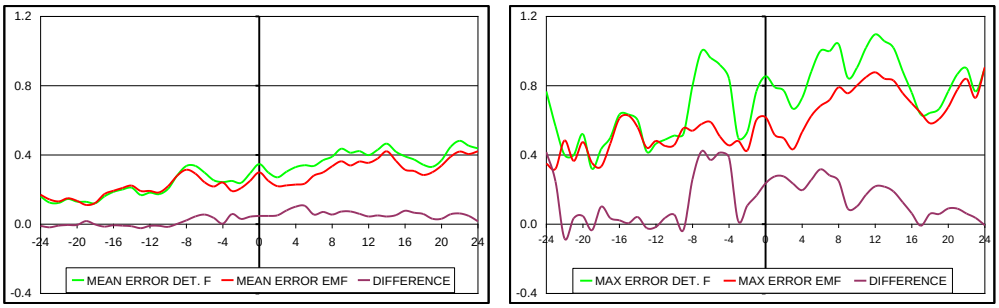

Figure 6 Mean (left panel) and maximum (right panel) error of the ten normalized events for the 24hour forecast. The lines refer to the EMF (red), the DF (green) and to their difference (error of DF minus error of the EMF, brown line). The time 0 refers to the time of the observed SL peak.

3.4.3 Probabilistic forecast information

The main goal of EPS is to provide an estimate of the forecast error and of the probability of exceeding fixed threshold values. Only in one of the 10 events considered in this study (both for the 24, 48 and 72 hour forecast) the observed maximum SL was outside the range of values produced by the EPS. Therefore, with only one exception, the observed peak was always within the range of the possible values produced by the EPS and a non nil probability was therefore assigned to reaching the peak. Fig. 7 shows an example of probabilistic prediction for the 24 hour EPS of event n° 10, which assigned a 10% probability of a SL peak higher than observed (72cm, left panel). Note that the maximum probability (0 CET on 24.12.2012) of reaching such threshold does not coincide with the maximum of the EMF (12 CET on 23.12.2012), because in this case the increase of the spread of the EPS has a larger effect than the variation of the its mean value. The right panel shows the equivalent information for the total sea level and a large (140cm) threshold. The effect of the astronomic tide on SL can change significantly the periods during which the probability of exceeding a given threshold is larger than 0 (comparison between 0 CET on 24.12.2012 and 12 CET on 23.12.2012 for the probability to exceed 140cm).

Of course probability can be computed for any SL values at a fixed time.

Fig.8 shows, according to the 48hours forecast, the probability of exceeding a SL threshold (x-axis) at 0 CET on 24.12.2012 EPS forecast of event n.10. The figure reports also the actual values of the deterministic forecast (green bullet), EMF (red bullet) and the observed value (blue bullet). The observed value (134cm) was within the predicted range with an (approximately) 10% probability of exceeding it.

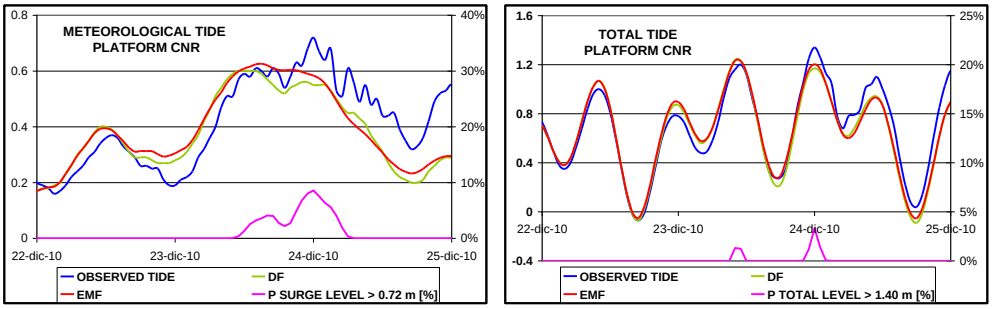

Figure 7 Event n.10. Left panel: sea level (left y axis, m) of 48 hour DF (green line), EMF (red line) observed level (blue line) and probability (violet line, right y-axis , %) of exceeding the observed peak level (72cm). Right panel shows the equivalent information for the total sea level same information for the total sea level (including astronomical tide) and probability of exceeding 140cm level (threshold above which approximately 60% of the city is flooded).

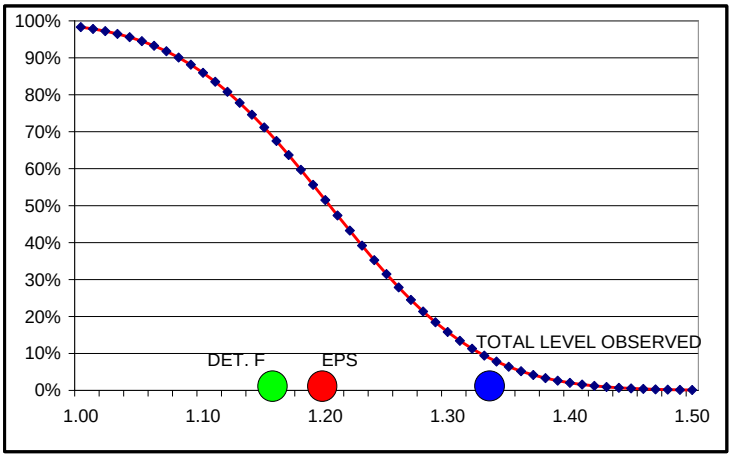

Figure 8 Probability (y-axis) of exceeding a total sea level threshold (x-axis) at 0 CET on 24.12.2012 for the 48hours EPS forecast of event n.10. The figure reports also the actual values of the deterministic forecast (green bullet), EMF (red bullet) and the observed value (blue bullet).

3.4.4 Accuracy of the EPS probability distribution

Though, because of the small set of events considered in this study , the evaluation of the accuracy of the EPS probability distribution has a limited statistical value, some analysis has been, anyway, computed.

Fig.9 shows the rank histogram (sometimes called a Talagrand diagram, Anderson 1996, Hamill and Colucci 1997, Talagrand et al. 1997) for the 24 (red bars), 48 (green bars) and 72hours (blue bars) forecast and their sum. The bars represent the position of the observed values with respect to the 50 members of the ensemble. Bars that are located after position 50 indicate observations larger than any member of the ensemble. Observations smaller than any member of the ensemble never occur. In an ideal EPS system, the actual evolution should correspond to a generic member of the EPS system and the observed peak value should be equally likely to have any rank within the peak values of the EPS members. In this ideal case the bars representing the observed values should be equally distributed among the bins in the x-axis. Instead, Fig.9 shows that the observations are more likely to lie at the highest ranks and the EPS system has a negative bias.

The negative bias is further confirmed by Fig.10 which shows the statistical distribution of the normalized index $\overset{*}{P}_k^i$ for SL peak values:

$$\overset{*}{P}_k^i = \frac{P_k^i - \mu_i}{\sigma_i} \tag{11}$$

where P_k^i is the peak value in the i-th member of the EPS in the k events, μ_i and σ_i are the EMF and standard deviation of peak values for

the k-th event. The normalized indexes follow the Gaussian distribution with a 0.95 confidence level according to the χ^2 test statistics. Fig.11 reports also the 10 observed normalized peak indexes (computed using for each event the respective μ_i and σ_i) and the Gaussian distribution with their mean and variance. The comparison confirms that the EPS distribution is affected by a negative bias and, further, suggest that it is too narrow. Therefore it is expected to underestimate the uncertainty of the forecast.

A well known metrics for the validation of the EPS results is the Brier score (BS, Brier 1950) though in our case its relevance is weakened by the small size of the sample. Further, when applied to the peak index $\overset{*}{P}_k^i$, the results are in the peculiar situation that all observed values are 1 and therefore in the BS formula

$$BS(\overset{*}{h}) = \frac{1}{N}\sum_{k=1}^{N}(p_k(\overset{*}{h}) - o_k(\overset{*}{h}))^2 \qquad (12)$$

where N is the number of events, $p_k(\overset{*}{h})$ and $o_k(\overset{*}{h})$ are the probability of a surge higher than according to the EPS and to observations, respectively, $o_k(\overset{*}{h})$ is 1 for $\overset{*}{h} \le 1$ and 0 otherwise. The interpretation of BS (Fig.11) is that the EPS computes well the probability only of forecasts 10% higher or 40% lower than the observed ones.

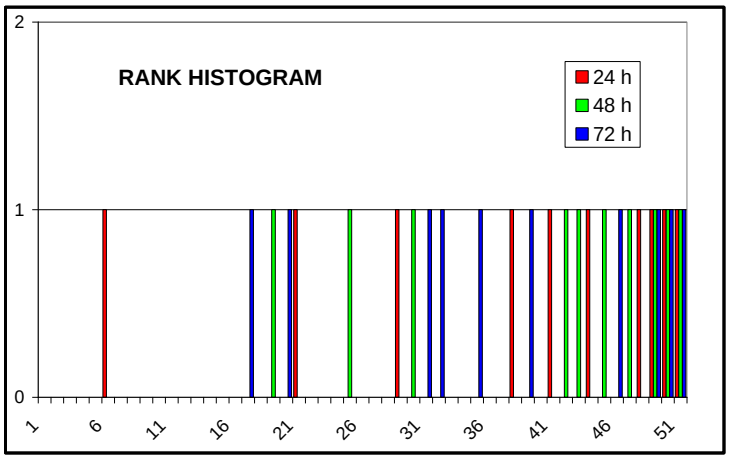

Figure 9 Rank histogram (Talagrand diagram) for the 24 (red bars), 48 (green bars) and 72hours (blue bars) forecast.

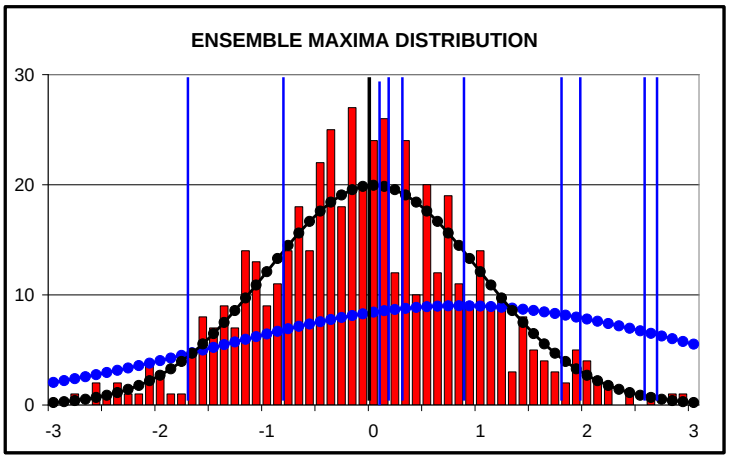

Figure 10 Distribution of the peak indexes (red bars) with the respective Gaussian distribution (black dotted line) for the 24 hours forecast. The blue bars show the observed peak indexes and the blue dotted line is the Gaussian with their mean value and standard deviation.

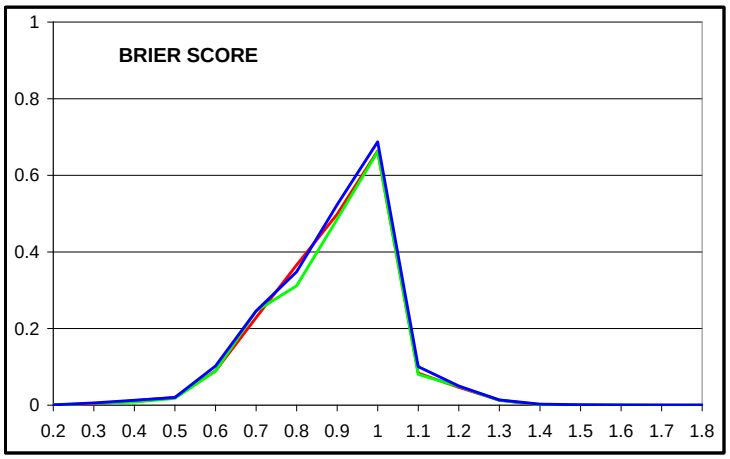

Figure 11 Brier score for the 24 (red bline), 48 (green line) and 72hours (blue line).

3.4.5 Comparison with the statistic model

To complete and make more robust the analysis the same ten events, which occurred in 2009 and 2010, are simulated with the statistic model IS08. For each event four set of 50 different SL forecasts are produced by that model, based on the EPS fields (the same used in HYPSE forecast). The four set differ from the number of gauges that uses ensemble data: in the first set all the forecast data in the four points are obtained from ensemble, in the second set only the data in CNR platform are ensemble, in the other three gauges (Genoa, P. Torres and Bari) observed data are used for forecast. The third set differ from the second because also for pressure in CNR platform observed data are used (only wind in CNR platform change in every ensemble forecast), finally the fourth set is the opposite of the third: it uses observed wind and ensemble pressures for every gauge. Four set are used to study possible differences in reliability of forecast and in its uncertainty.

The IS08 model is exactly the same in all 200 forecasts, which for sea level and current adopt the same initial condition, which is obtained from the

observed pressure, wind and tide value in the 24 hours before the forecast . In other words, each set of the 50 simulations is made on a one day analysis (identical for all 50 simulations) and a three day forecast, each presenting a different sea level evolution because of the 50 different forcing.

The analysis of the results is based on comparing the model 5 minutes data with the hourly observed SL at Punta Salute (PS) gauge, located in the centre of Venice in front of San Marco square. For each event 2 prediction ranges have been considered, corresponding to forecast launched at 00 UTC, approximately 24 and 48 hours before the observed peak of sea level. Therefore the study is based 10x2x50x4 simulations of IS08. Each simulations reproduces the meteorological contribution and the following seiches, which have no appreciable nonlinear interaction with the astronomical tide, which has to be added for obtaining the actual SL, as was done for the HYPSE results analysis.

As done with deterministic model, it has been decided to normalize the time series, to reduce them to a dimensionless index which facilitates their comparison, however in this model analysis R, the background value which is meant to account for the mean SL of the Adriatic at the onset of the event, described in cap. 3.4.1, is zero, because the value at the beginning of the forecast is imposed as the observed PS value. Moreover, the model consider also gauges out of the Adriatic Sea, that take in account the possible transfer of water mass through Otranto channel. The following comparisons of IS08 output consider almost always normalized time series.

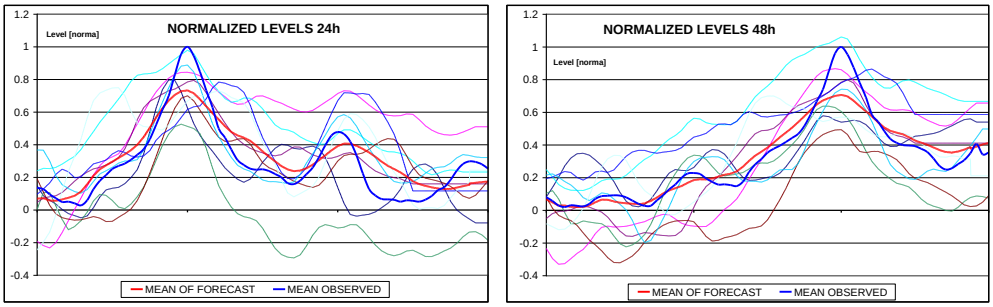

Figure 12 Evolution of the mean normalized time series of the ten events listed in table I considering the 24h and 48h forecasts and the time range from the beginning of forecast to the end of model run (72h). The mean observed SL at the CNR platform (blue line) and the EMF simulations (red line) are shown, when the all forecast data come from the ensemble forecast.

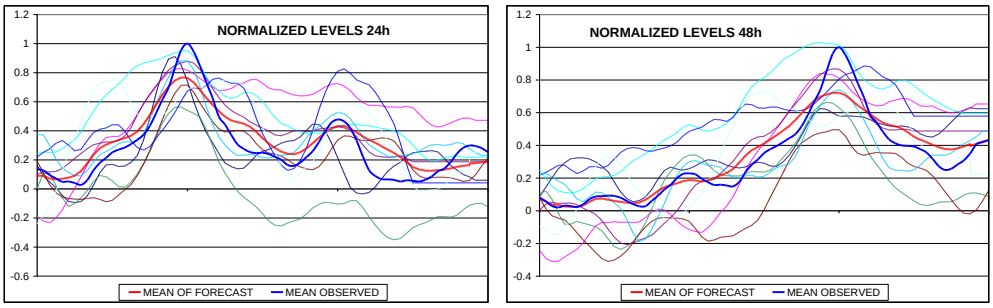

Figure 13 The same of Fig.12, but the parameters change only in CNR platform, in the other gauges observed pressure data are used for the all 50 forecasts.

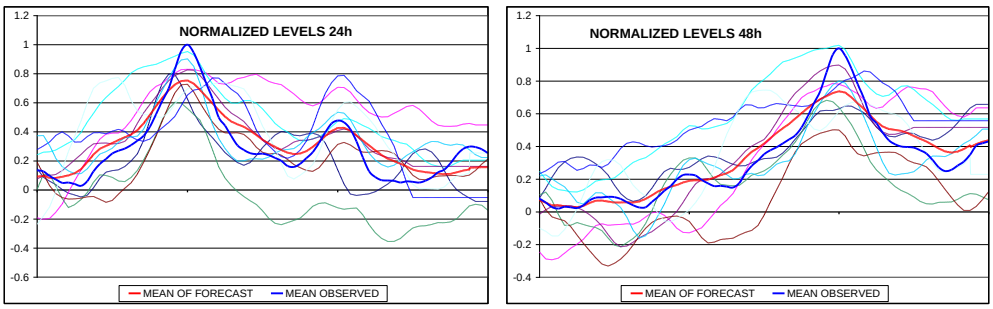

Figure 14 The same of Fig. 13, but also the pressure data in CNR platform doesn't change.

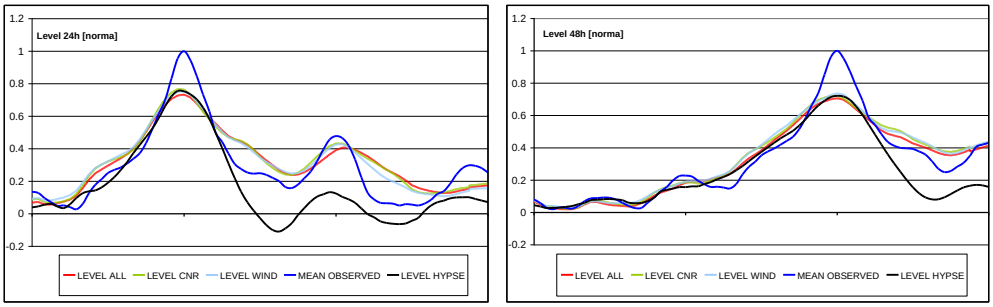

Figure 15 The graph summarizes the ensemble mean level forecast represented in Fig.12-14: no significant changes are detected on the mean.

3.5 Evolution of the spread in the EPS

In order to study the behaviour of forecast uncertainties is basic to understand the behaviour of variance. The aim is to study its trend in function of time and the synchronism between surge peak and tide variance. More important is to find a relation between tide and meteorological variance to provide the first directly from the meteorological field.

3.5.1 Variance analysis

Fig.16 shows the dependence of the mean absolute error of the DF, ensemble mean, standard deviation and mean spread (mean of 10 events of highest minus lowest value in the ensemble) with the forecast range (for the 24, 48 and 72 hour forecasts). With increasing time range the error (a negative bias) increases slightly, but the spread increases at a higher rate so that the estimated probability of a peak level above the observed one increases.

The spread among EPS simulation represent a measure of the uncertainty of the prediction it should present a statistical relation with the error, so that cases with the larger spread are those with highest uncertainty and therefore where an error of the ensemble mean (and also of the deterministic forecast)

is more likely. In our case only 10 events are available and the statistics is not robust, however fig.17 show some tendency of the error to increase with the spread for all forecast ranges.

The time of storm surge peak corresponds to maximum of SL uncertainty. Fig.18 shows the time evolution of the normalized variance for the 10 EPS. Different time ranges have been considered and for each event the value of the variance have been normalized with the mean value during the whole simulation. Time series have been shifted in time so that the peak of the surge occurs at 24, 48, 72, 96, 120 hours in the different panels, corresponding to forecast launched approximately 1, 2, 3, 4 and 5 days before the surge maximum, respectively. Fig.18 clearly shows that uncertainty reaches a maximum at the time of the SL peak and that the maximum uncertainty increases approximately linearly with the forecast time range (panel f). The blue line in Fig.18f represents the mean of all red lines and can be considered (approximately because it includes for one time series out of six also the day with the peak) the mean value of the spread without the storm surge event. Fig.18f shows clearly that storm surge events correspond to uncertainty maxima whose level increases with time.

Fig.19 is produced adopting a different time shift with respect to fig 18 so that the maximum of the spread occurs at 24 and 48 hours in order to show that uncertainty oscillates with a period corresponding to that of the main seiche of the Adriatic basin (22hours, approximately). This is an effect of the dynamics of the storm surge model.

In order to investigates the causes for the uncertainty of the forecast the standard deviation of the SL peaks has been compared (Fig.20) with that of the MSLP and wind speed at platform CNR (fig.1). The variances of wind

speed and MSLP have been normalized with the same criterion as for the SL. The variance of the SL follows very closely that of the wind speed for the 24, 48 and 72 hour forecast, at difference with the 120 and 144hour forecast during which it follows that of the MSLP.

These results show that the quasi-linear dynamics of storm surge in the Adriatic Sea does not add further uncertainty to that of the meteorological forecast and the maxima of uncertainty at the time of the SL peak are the effects of maxima of uncertainty of the meteorological forcing fields.

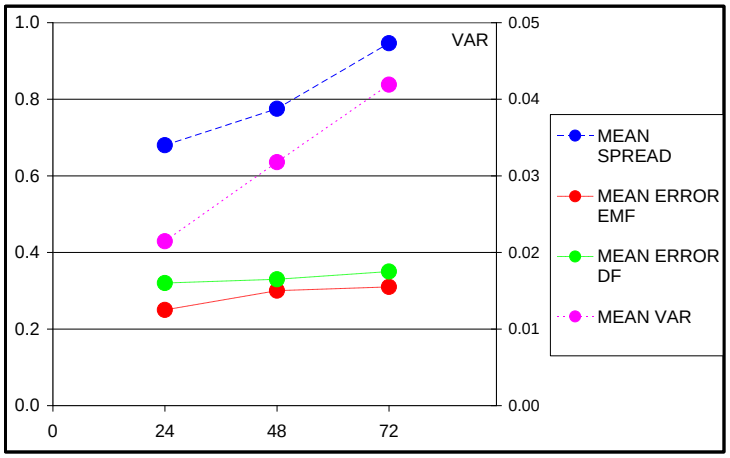

Figure 16 Mean absolute error of the deterministic forecast (green), of the ensemble mean (red), standard deviation of the EPS (pink) and its spread, (blue) from the forecast launched 24, 48 and 72hours before the peak.

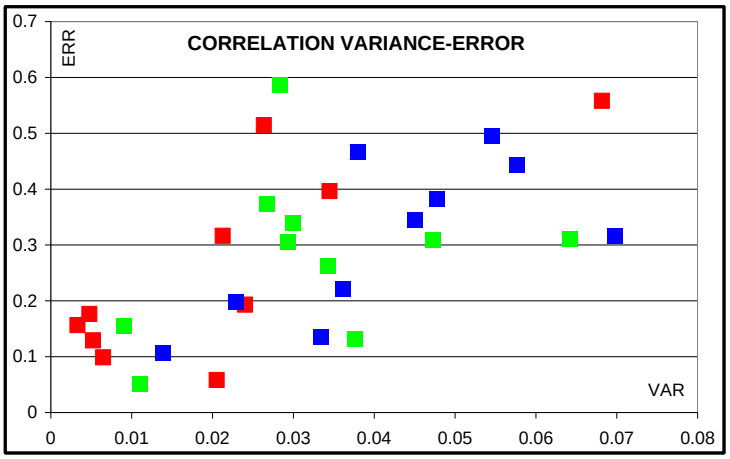

Figure 17 Scatter plot of the absolute error of the ensemble mean (y-axis) versus the spread of the Ensemble (x-axis) the 24 (red), 48 (green) and 72hours (blue).

a b

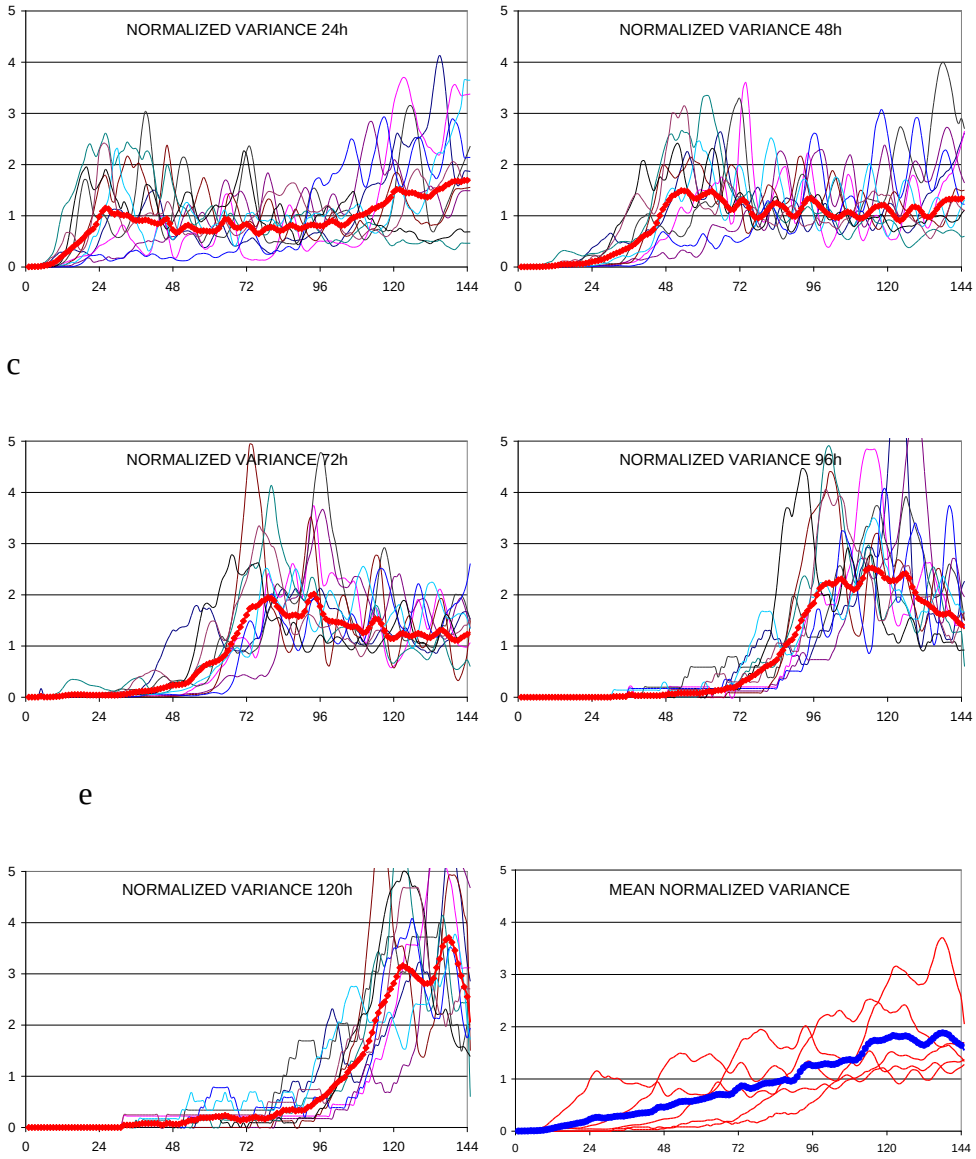

c d

e f

Figure 18 Panel a-e: evolution in time of the mean-normalized variance with time range. Colour lines represents the single event, the red line their mean value. Panel f reports the red lines of panels a-e and their mean (blue line). A time shift has been applied for each event, so that the peak is reached at 24, 48, 72, 96, 120 hours in panels a to e respectively.

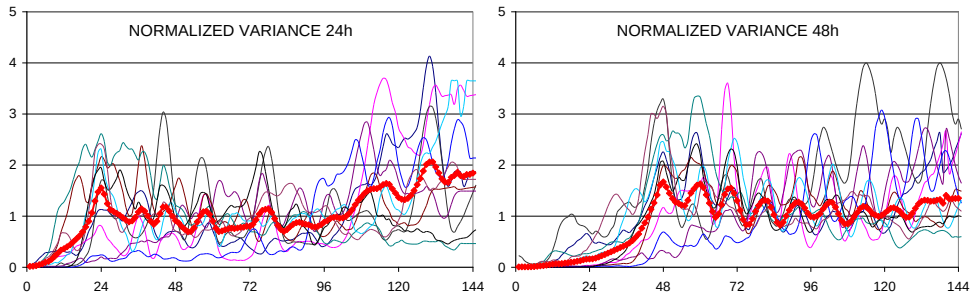

Figure 19 Evolution in time of the normalized variance with a variance peak time-aligned: oscillations with seiches-period could be seen in both 24 and 48 hours forecast.

a b

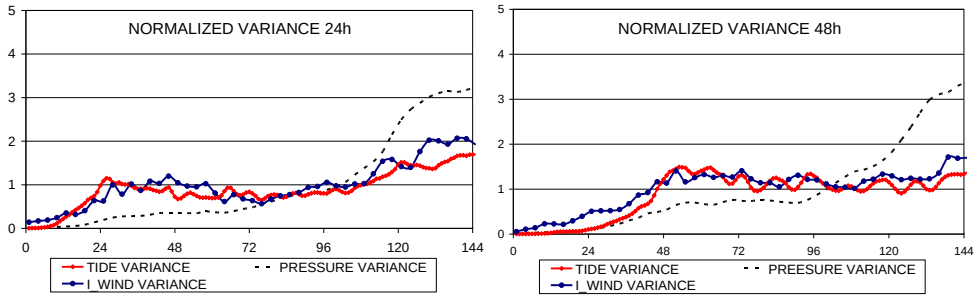

c d

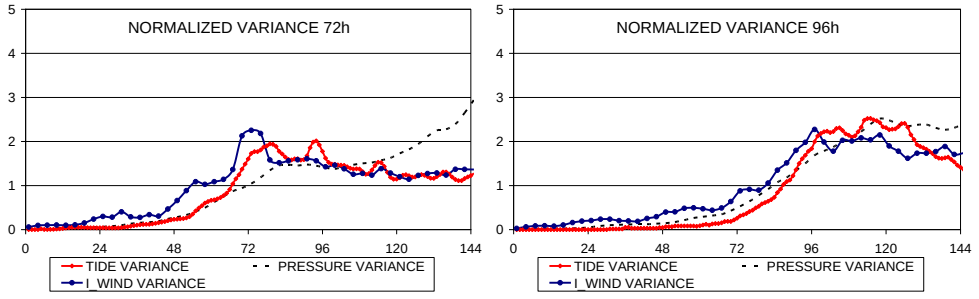

e f

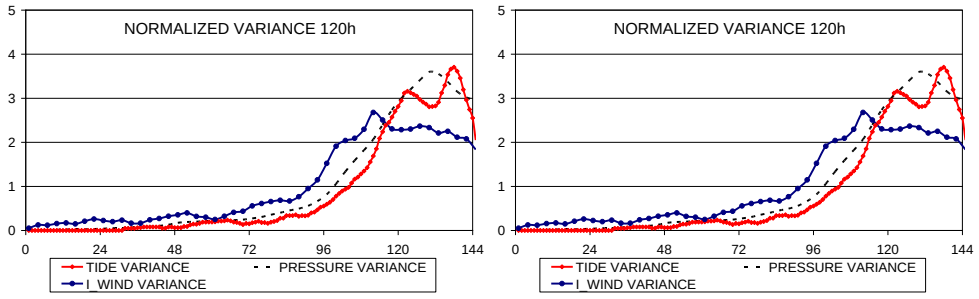

Figure 20 Comparison of the evolution in time of SL normalized variance (red line) and of the variance of the meteorological forcing (blue line for wind and black line for pressure). Panel f shows the mean trend.

3.5.2 Comparison with the statistic model

The results obtained from the statistical model are very similar to HYPSE variance trend. Fig.21-23 shows the time evolution of the normalized variance for the 10 EPS. For each event the value of the variance have been normalized with the mean value during the whole simulation (with level-normalized data) . Time series have been shifted in time so that the peak of the surge occurs at 24 and 48 hours in left-right panels, corresponding to forecast launched approximately 1 and 2 days before the surge maximum, respectively. In Fig. 21 the results using the ensemble fields (pressure in CNR platform, Genoa, Bari, Porto Torres and wind in CNR platform) in all gauges are shown. Fig. 22 shows the results using ensemble fields only in CNR platform, finally in Fig.23 the model run with ensemble data only for the wind and the observed values for pressure forecast. Fig.21-23 clearly show that wind uncertainty reaches a maximum at the time of the SL peak; fig. 24 shows a lower relationship between pressure and surge variance . Fig. 21-24 show a variance increasing from 24 to 48h of forecast.

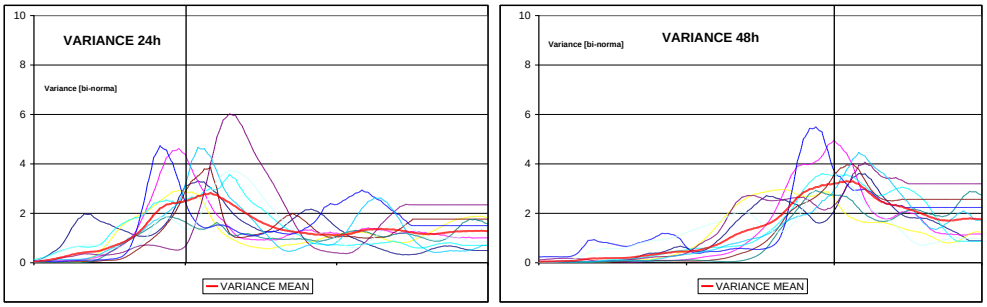

Figure 21 Evolution in time of the mean-normalized variance with time range. Colour lines represents the single event, the red line their mean value. A time shift has been applied for each event, so that the peak is reached at 24 and 48 hours respectively. In these figure the all forecast data come from the ensemble forecast.

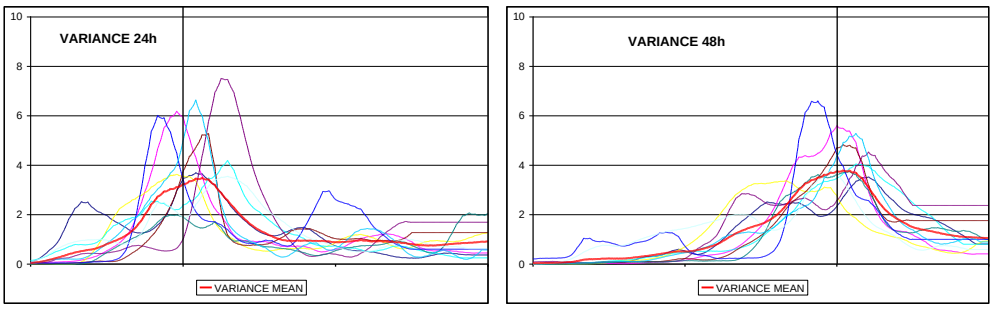

Figure 22 The same of Fig.21, but the parameters change only in CNR platform, in the other gauges observed pressure data are used for the all 50 forecasts.

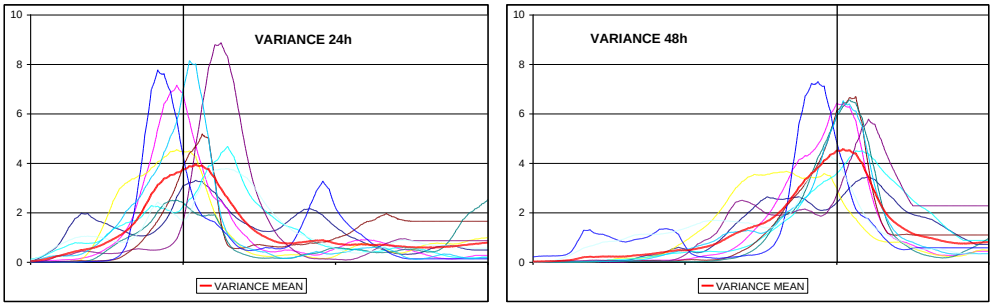

Figure 23 The same of Fig. 22, but also the pressure data in CNR platform doesn't change.

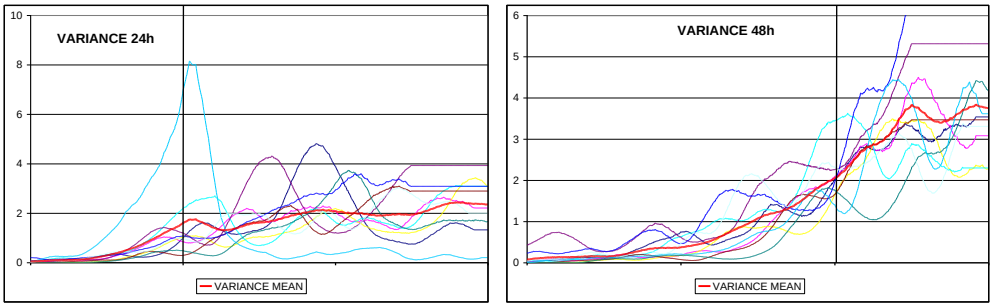

Figure 24 The same of Fig.21, but the parameters change only for pressure data

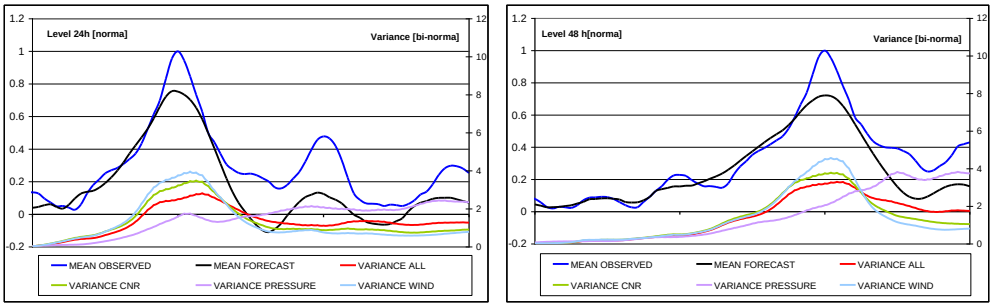

Figure 25 The graph summarizes the ensemble mean level forecast represented in Fig.21-23: the variance grows increasing the number of parameters got from the ensemble fields.

3.6 Prediction of the spread

Tide spread is of paramount importance for probabilistic forecast, because permit to compute its uncertainty and the probability to reach an interesting value.

The best solution in a surge probabilistic forecast is to compute a single high resolution forecast (the best forecast now available) and then to define the uncertainty through the variance, in the fastest computational way.

One choice is to define the surge variance from the meteorological variance, using the same gauges of the statistic model IS08: a linear

regression is computed using seven parameters: six pressure gradients between the four IS08 gauges and the CNR platform north-east and south-east winds. Fig. 26 shows a good surge variance (normalized with its forecast-series mean) predictability from a linear combination the seven parameters, for both 24 and 48 hours forecasts.

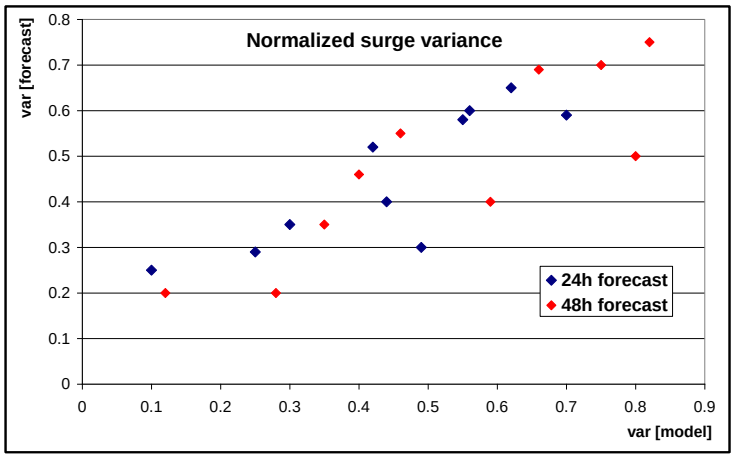

Figure 26 Scatter plot of the variance computed by linear seven parameters combination (y-axis) versus the variance computed from the tide outputs of the statistic model IS08 (x-axis) for the 24 (blue) and 48hours (red).

3.7 Conclusions

Ensemble forecasting aims to improve the quality of risk management decisions by using multiple forecasts to quantify the forecast uncertainty. This work focus on the construction of an ensemble forecasting system for Northern Adriatic Sea storm surges, believed to be regularly run and used. By propagating the consequences of atmospheric uncertainty through to impact-related variables, it is hoped that such systems make ensemble forecasting more relevant and useful to emergency responders. An EPS for storm surges in the Northern Adriatic has been implemented using the

ECMWF EPS for the wind and MSLP forcing fields. The analysis of the results is focused on the peak values (and not on hourly values) of relatively intense events, which occurred in the period 2009-2010. Clearly this study is not conclusive because simulating the operational practice and collecting a much larger set of events is needed for more robust conclusions. However, this analysis has already produced interesting outcomes.

The EMF has an accuracy slightly higher that the single DF for predicting the peak SL values. It is also more robust, meaning that hourly prediction have a slightly lower mean error and a much lower maximum error during the day before and after the peak.

The EPS probabilistic forecast is biased low and underestimates the uncertainty of the forecast. The low bias is inherited from the deterministic prediction. It is reasonable to expect that these problems of the probability distribution (negative bias and low spread) can be mitigated with simple first and second moment corrections based on adequate sample size.

The EPS spread increases linearly with time and it is proportional to the spread of the forcing fields. The quasi-linear dynamics of storm surge in the Adriatic does not add uncertainty to the SL prediction, which is mainly determined by that of the weather forecast, which has a maximum at the time of the storm peak. The main resonant mode of the basin (22-hour seiche) adds the corresponding periodicity in the EPS spread.

Moreover, the EPS spread is correlated to the error of the EMF, meaning that EPS with large spread not only are more likely to produce a wrong EMF, but also the corresponding DF will be more often wrong.

Finally the HYPSE and IS08 variance results are practically the same: this makes more robust the study and permits to compute the variance in few minutes not only running the statistic model but also directly from the pressure and wind fields, using a simple linear regression.

4. Future surge statistic

In this study a future storm surge scenario is evaluated using new high resolution sea level pressure and wind data recently produced by EC-Earth (see cap. 2.2.2) The study considers an ensemble of six 5-year long simulations of the rcp45 scenario at 0.25º resolution and compares the 2094-2098 to the 2004-2008 period. EC-Earth sea level pressure and surface wind fields are used as input for the shallow water hydrodynamic model HYPSE (see cap 2.3).

4.1 Method

For this study, data from an LRV simulations covering the period from 1850 to 2100 have been extracted. This simulation uses the observed climate parameters from 1850 to 2005 and the rcp45 emission projections for the period 2006 – 2100. The large computing time needed to run HRV has prevented so far to reproduce the whole 1850-2100 period. This study uses two ensembles of HRV: six 5-year ensemble runs of the present climate (2004 – 2008) and of the rcp45 scenario (2094 – 2098) have been performed. Therefore, 30 years are available at high resolution for both the present climate and the rcp45 scenario.

The storm surge model runs have been carried out using both LRV and HRV forcing. When using the LRV forcing, decadal statistics of sea level for periods from 1850-2000 (past climate) and 2010–2100 (climate scenario) have been produced. When using the HRV forcing, 30-year (i.e. six 5-year long simulations) statistics of sea level both for the present (2004-2008) and the future (2094-2098) scenarios have been computed.

The sea level statistics consider the number of hours above/below levels separated by 0.05m steps, starting from 0.00 m, for 4 points in the Adriatic Sea. The first and the most important is the tide gauge located 15 km offshore the Venice Lagoon on platform ISMAR-CNR (45°19' N; 12°30' E), where a long time series of hourly sea level observations is available. The other points are situated in Trieste, Rovigno and Ancona (Fig. 27, left panel). Fig. 27 on the right panel show the points where meteorological components are compared.

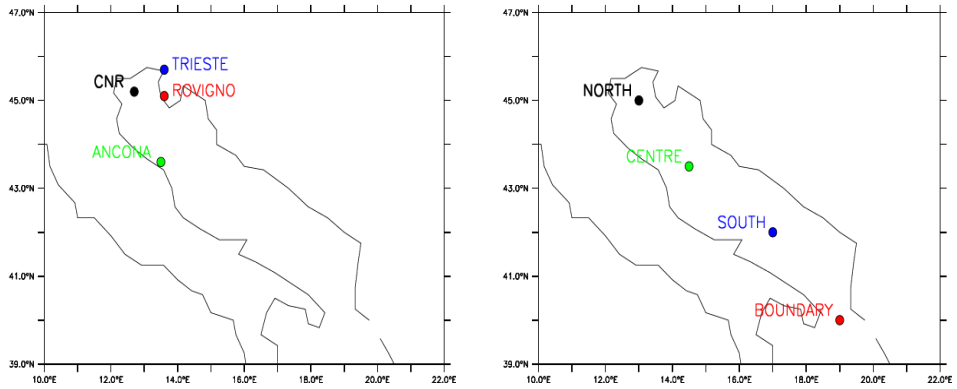

Figure 27. Adriatic sea with the points used for the tide (on the left) and wind - pressure (on the right) statistics comparisons: they cover the whole Adriatic sea. For pressure statistics a point in the boundary (Otranto Channel) is useful to compute the pressure difference between CNR platform and the southern edge of the basin.

Statistics were also computed for the number of storms. A wind storm is here defined as time duration of at least 30 hours during which the wind speed exceeds a fixed level. The cumulative distribution has been computed considering progressively increasing wind speeds from 10 m/s separated by 1 m/s steps. A similar concept is used for sea level pressure and sea level considering steps of 2 hPa and 0.05 m, respectively.

4.2 Model validation and importance of resolution

Model results are compared with observed statistics of sea level data from the tide gauge located outside the Venice Lagoon at CNR platform for the period 1974-2010 (Figure 28). The influence of the sea level variations originating outside of the Adriatic Sea (about 0.05 m for the periods with surge > 0) has to be subtracted from the observations to make the data comparable to the model output. A preliminary analysis has shown that decadal surge statistics produced with the LRV forcing show no trend over the whole 1850-2000 period therefore, results from the whole period have been used to describe present conditions. For the HRV, the analysis uses the total of 30-years from an ensemble of six 5-year long simulations. The 10 year time offset between HRV and LRV and the larger time offset with respect to observations is considered irrelevant because of the steadiness of statistics in LRV.

Figure 28 shows that forcing the surge model with low resolution input meteo fields does not produce adequate statistics of sea level in the Northern Adriatic Sea, especially high sea level values. In LRV-forced simulations no sea level higher than about 0.80m occurs, while in observations this threshold is reached for about 200 hours per decade. HRV-forced simulations show a better statistics than LRV forced simulations and looks more reliable for simulating present and future sea level extremes.

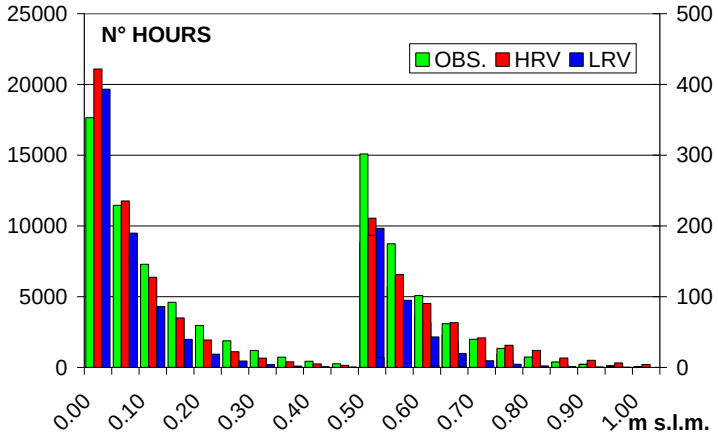

Figure 28. Cumulated number of hours per decade of water level above fixed thresholds (x-axis) at the ISMAR-CNR platform. HRV and LRV simulations are compared with the observations of the period 1974-2010. The enlarged scale on the right is used for sea levels >0.50 m.

The shortcomings of LRV sea level statistics can be traced back to those of winds. In Fig.29 (left panel) LRV and HRV statistics are compared with ERA-Interim reanalysis (Dee et al. 2011) wind data, considering the south-east component, which is the main factor producing Venice floods. Results show that high resolution is fundamental for approximating the wind speed distribution of ERA-Interim. Conversely, mean sea level pressure values (Fig.29 right panel) are not critically sensitive to the model resolution. This confirms several previous studies on the importance of resolution for correctly modelling wind speed (e.g Cavaleri et al. 2000, Lionello et al. 2003).

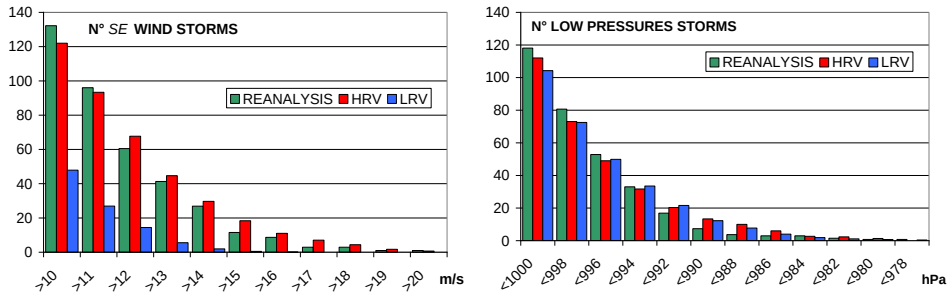

Figure 29. Number of south east wind-storms per decade (left panel) and number of hours per decade below a low-pressure threshold (right panel) for the HRV and LRV simulations and ERA-Interim at the ISMAR-CNR platform.

4.3 Results

In this section a systematic analysis of climate change signal is carried out by comparing sea level pressure, wind and sea level cumulated frequency distributions of the HRV simulations in the 2094-2098 and 2004-2008 periods. Statistical significance of differences is assessed with the t-test estimating the degrees of freedom with the Welch-Satterthwaite approximation (Motulsky 1995). As a guideline, for Gaussian variables, t values larger than 4, 2.5, 2 imply a 99%, 95% and 90% confidence level, respectively.

4.3.1 T-Test

The two means $\overline{Y}, \overline{Z}$ that are compared can be considered as two random samples of measurements, represented by

$$Y_1,...,Y_n \text{ and } Z_1,...,Z_n \tag{13}$$

where the Y's are sampled from process 1, the present-day statistics, and the Z's are sampled from process 2, the future statistics. Both processes are considered independent. We test if the mean values of the two processes are

the same or if some trend appears. The basic statistics for the test are the sample means the sample standard deviations S1 and S2 with degrees of freedom ν1=N1-1 and ν2=N2-1 respectively (Harvey J. Motulsky 1995).

Because it cannot be assumed that the standard deviations from the two processes are equivalent, the test statistic has the following form:

$$t = (\bar{Y} - \bar{Z}) / \sqrt{((\frac{S_1^{\ 2}}{N_1}) + (\frac{S_2^{\ 2}}{N_2}))} \tag{14}$$

The degrees of freedom are not known exactly but can be estimated using the Welch-Satterthwaite approximation

$$\nu = ((\frac{S_1^{\ 2}}{N_1}) + (\frac{S_2^{\ 2}}{N_2}))^2 / (\frac{S_1^{\ 4}}{N_1^{\ 2} \cdot \nu_1} + \frac{S_2^{\ 4}}{N_2^{\ 2} \cdot \nu_2}) \tag{15}$$

The strategy for testing the hypothesis is to calculate the appropriate t statistic from the formulas above (Harvey J. Motulsky 1995), and then perform a test at significance level α, where α is chosen to be small, typically .01, .05 or .10. The hypothesis associated is rejected if:

$$|t| \geq t_1 - \frac{\alpha}{2}, \nu \tag{16}$$

The critical values from the t table depend on the significance level and the degrees of freedom in the standard deviation. For hypothesis t1-α/2, ν is the 1-α/2 critical value from the t table with ν degrees of freedom.

4.3.2 Climate change impact on sea level pressure

Pressure statistics have been computed at four points along the axis of the Adriatic (Figure 27, right panel). Figure 30 shows the t-test statistics for the number of hours above fixed thresholds and shows a very significant increase of high pressure periods (>1015 hPa) and a significant increase of

pressure level from 1000 hPa to 1015 hPa. Figure 31 shows the cumulated number of pressure events below fixed thresholds (left panel) and of high pressure events above fixed thresholds (right panel). A t-test (not shown) reveals no significant differences for the storm distribution and a very significant increase of high pressure events. Finally, Figure 32 compares the frequency distribution of the pressure difference between the ISMAR-CNR platform and the southern boundary of the Adriatic Sea, and shows an increase of conditions with large positive and negative pressure differences.

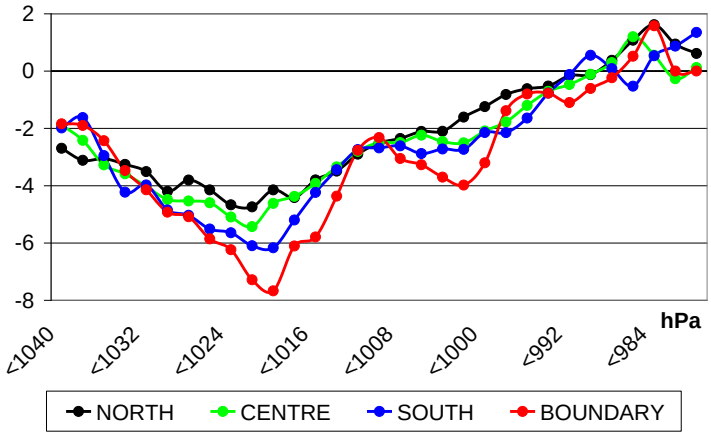

Figure 30. t-test values for cumulated distribution of number of hours below fixed thresholds with 2 hPa-step from 980 to 1040.

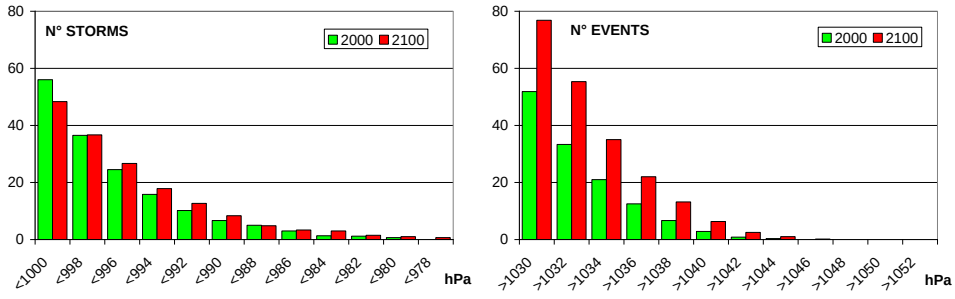

Figure 31. Cumulated distributions of pressure events below fixed thresholds (left panel) and high pressure events above fixed thresholds (right panel) at the ISMAR-CNR platform.

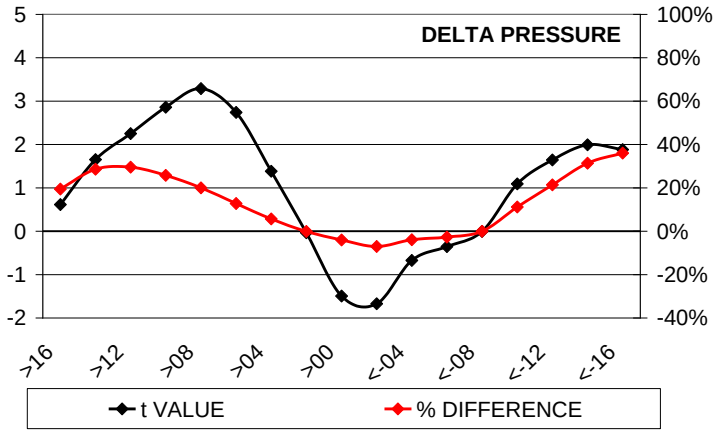

Figure 32. t-test (black line and left-axis) for number of hours per decade as function of the pressure difference between the Northern part and the southern boundary of the Adriatic Sea. The red line (right axis) shows percent difference in the number of hours

4.3.3 Climate change impact on wind

For wind 12 different directional sectors are considered, each 30 degrees wide, and statistics are computed separately for each sector at three points along the Adriatic Sea (labelled north, centre and south Adriatic in Figure 27). Fig. 33 shows the t-test statistics for the number of hours above fixed thresholds (left column) and the number of storms above the same thresholds (right column). The upper row considers all wind directions, the middle and lower rows consider only north-easterly (bora) and south-esterly (scirocco) winds, respectively. These directions have been chosen because they cause most of storm surges in the Adriatic Sea (particularly the south-esterly winds). A significant decrease of conditions related to low and moderate wind speed (up to 12 m/s) is found for all directions. However, the difference associated with high wind speed conditions, which are expected to be responsible for high storm surges, are not statistically significant and in

general all other changes are below the commonly accepted minimum 90% confidence level.

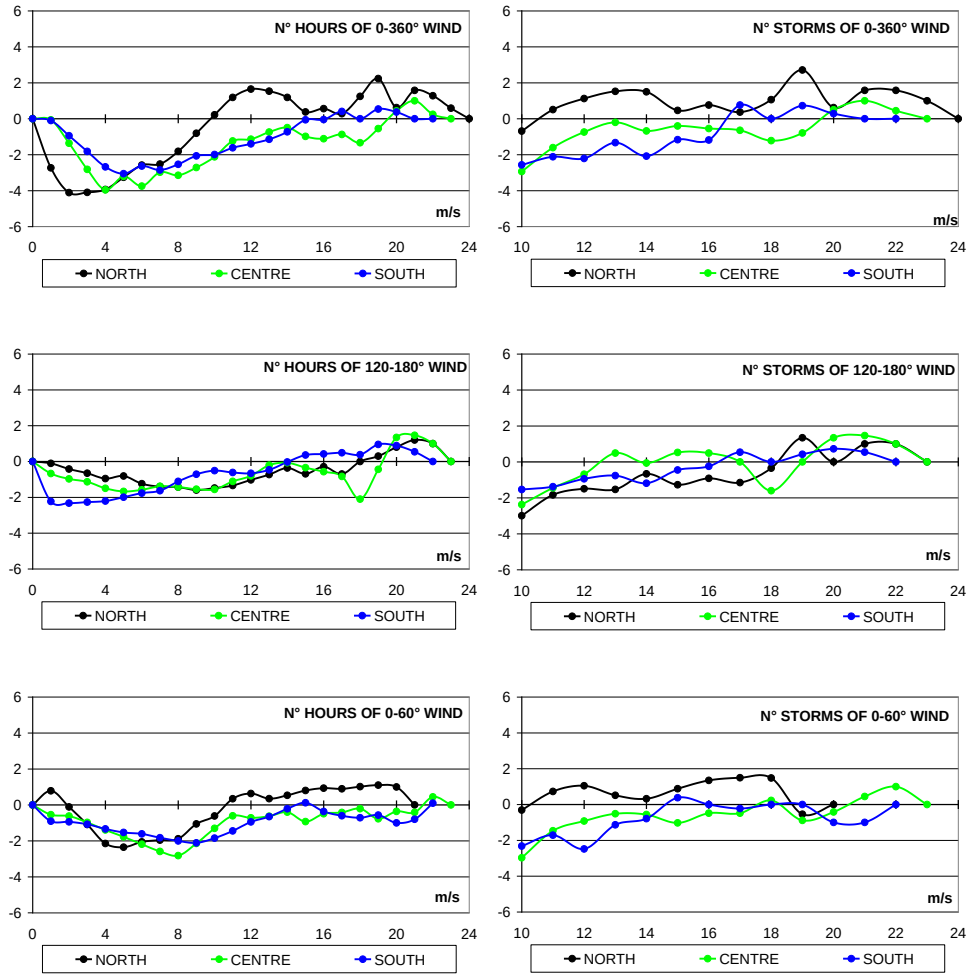

Figure 33. (panels a-f) t-test for cumulated number of hours above fixed wind speed thresholds (left side column,) and for the number of storms (right column) at the North, Centre and South points in Figure 1. Upper row considers all wind directions, central row considers south-easterly winds (120°-180°), bottom row north easterly winds (00°-60°).

4.3.4 Climate change impact on sea level

For water level we compare the mean of the five-years ensemble HRV runs at present with the same runs at future time. This is done for the whole level-step range and all stations. The same comparison is made for the number of storms above every fixed level.

Figure 34 shows the cumulated distribution of the number of hours (left panel) and number of storms (right panel) above-below fixed sea level threshold in present and future climate conditions at the ISMAR-CNR platform. No difference between present and future climate condition is statistically significant, not even with a low confidence level (less than 90%). Figure 35 shows the t-test at the four station in Figure 1a and suggests that no climate change signal in sea level is present in these simulations.

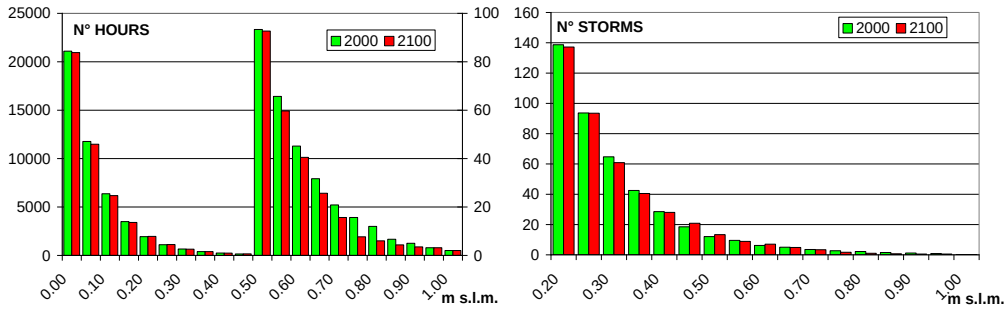

Figure 34. Cumulated distribution of the number of hours (left panel, the enlarged scale on the right is used for sea levels above 0.50m) and number of storms (right panel) above-below fixed sea level threshold in present and future climate conditions at the ISMAR-CNR platform.

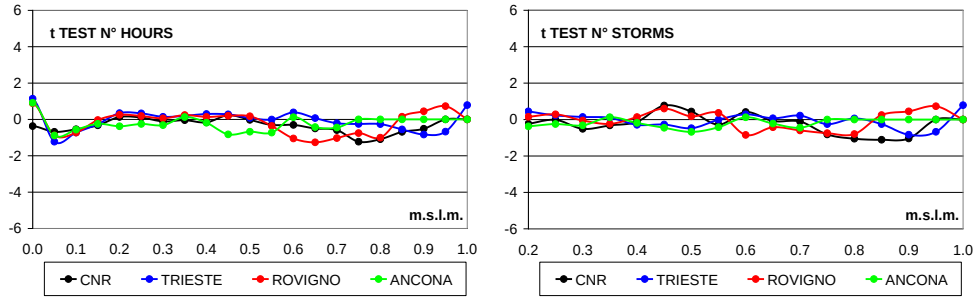

Figure 35. t-test for the cumulated distribution of the number of hours (left panel) above-below fixed sea level thresholds at the four locations shown in Figure 1a. Results for the number of storms (panel on the right) are about the same.

4.3.5 Climate change impact on rain

Rain statistics, divided in large scale and convective, are finally analyzed for to points: one on Venice and the second 100 km inland in the west side. The rain does not concurs directly to generate a surge, but gives more information about the storms trend.

In Fig. 36 on the left side the t-test trend (relative to Venice) from 0.1 mm/h to 10 mm/h is shown for large scale, convective and the sum of both kind of precipitations. As proved by other studies, the results show a decreasing of the number of hour (and consequently of days) of rain and also the quantity of light-rain (0-2 mm/h) hours, but an increasing of heavy (>3 mm/h) convective precipitations.

On the right side the graph show the yearly mean total precipitation in a present-time average compared with the future rcp45 scenario. It shows a decrease of about 5% for Venice and 10% for the point 100 km inland.

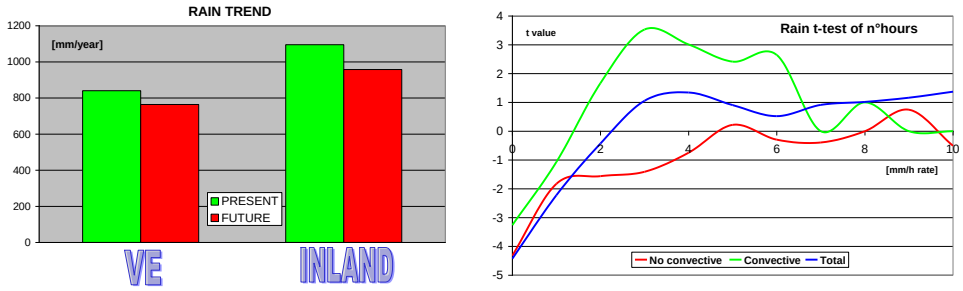

Figure 36. On the left the yearly rain mean is displayed for the gauges of Venice and a point 100 km inland from the coast with a decrease of 5 and 10%, respectively. On the right results of t-test for hourly precipitation 1mm-step from 0 to 10 mm/h. Large scale, convective and total precipitation are analyzed. The results suggest a decreasing of hours of rain and an increase of heavy convective precipitations.

4.4 Conclusions

EC Earth v. 2.3 data are used to analyze the climate difference for Venice and the Adriatic sea. Rcp45 scenario, using the High Resolution Version of the model is used, producing a six ensemble members of 5 years runs, both for the present (2004-2008) and for the future (2094-2098). Wind, pressure and rain fields are compared in their ensemble-mean distributions. The significance of differences is verified by a t-test. This is made at four points along the Adriatic sea, with a special care on meteorological situations favourable to storm surge in Venice lagoon. Then wind and pressure fields are used to run a hydrostatic tide model (HYPSE) working only in the Adriatic sea to see which could be the difference from present to the future in terms of tide storms, extracting the results for CNR platform (close to Venice and equipped of a long statistic series of observed data) and at three other points in the northern part of the Adriatic sea. Results show with a moderate certainty that surge statistics will not change if the simulated scenario happens. This is very important because Venice has not to manage also an

eventual increasing of number of storms, the statistic will change only due to the different scenarios of sea rising.

However this study proves that other parameters, like wind, pressure and rain, could change with the analyzed scenario. A decrease of total rain and windy periods is related to an increase of high pressure times, however the probability to have strong storm, wind or rain, does not change in a significant way: although a little increase is seen, the differences are not significant due to the variability of these events. To study them is necessary to produce a larger set of ensemble data, to get a better signal.

5. Conclusions

In this research a probabilistic surge forecast for Venice and a study for the future storm statistic evolution in the Northern Adriatic Sea are proposed.

EPS use gives considerable benefits in tide forecasting. It produces a second forecast, the EMF, that has a reliability equal to HRF but it can reduce the greater forecast errors. Moreover, looking the whole set of ensemble tide forecast and their variance, an idea of the possible surge evolutions can be developed. Finally to dispose a probability forecast can help both the its disclosure, that would be much simpler to understand by the citizens, and the strategy to manage close the inlet gates closing. Further developments to the operational probabilistic prediction procedure are certainly possible and recommended. They are related to the quantification improvement of the correlation between tide and meteo fields uncertainties, in order to estimate both spread and probability of error directly from the input fields, avoiding the computational weight of running 50 simulations. This problem could partially avoid computing the variance from the statistic model IS08.

Though improvements of the meteorological forcing, which is blamed for the poor performance of deterministic surge models, are certainly important this study shows that also a relatively cheap method is capable to improve the general quality of forecast, increasing the information useful to manage the increasingly frequent emergencies in city and lagoon of Venice.

New data from the high resolution global model EC Earth v. 2.3 (rcp 45) are used to analyze the climate change effect on storm surge levels at Venice and in the Adriatic Sea. The statistical significance of differences between future and present conditions is assessed by a t-test. Wind and pressure fields from the climate model simulations are used to drive a hydrostatic storm surge model (HYPSE) in the Adriatic sea to investigate the importance of the climate change signal for storm surge levels. Results for the CNR platform (close to Venice and equipped with a long series of observed data) and three other points in the northern part of the Adriatic sea are considered. Results show with a moderate confidence that storm surge statistics will not change in the simulated scenario. This confirms previous studies and shows that likely the main hazard to the north Adriatic flat coast and to Venice is posed by future sea level rise and not by an increasing number of storms. However, this study proves that other parameters, like wind and sea level pressure, are likely to change in future.

Future research should obviously consider simulations carried out with other climate models. Further, since the simulated scenario (rcp45) adopts a moderate increase of anthropogenic emissions, it is important to investigate other scenarios. An EC-Earth LRV simulation was performed adopting the rcp85 scenario which has a radiative forcing almost twice as large as rcp45 (if high resolution simulations will be available). LRV pressure analysis show that climate changes cause a twice as much effect with a rcp85 scenario than a rcp45: this could occur also for the wind and tide, but the resolution of that version is not enough to draw this conclusion.

6. References

Anderson JL. 1996. A method for producing and evaluating probabilistic forecasts from ensemble model integrations. *J. Climate*. 9: 1518−1530.

Brier GW. 1950. Verification of forecasts expressed in terms of probabilities. *Mon. Wea*. Rev.,78, 1–3.

Bajo, M., Umgiesser G. 2010. Storm surge forecast through a combination of dynamic and neural network models. *Ocean Modelling* 33: 1-9, doi: 10.1016/j.ocemod.2009.12.007.

Buizza R, Palmer TN. 1995. The singular-vector structure of the atmospheric general circulation. *Journal Atmospheric Science* 52: 1434–1456.

Buizza R, PalmernTN. 1999. 'Ensemble data assimilation'.In Proceedings of the 17th Conference on Weather Analysis and Forecasting, 13-17 September 1999, Denver, Colorado, US.

Bock, Y., Wdowinski, S., Ferretti, A., Novali, F., Fumagalli A., 2012. Recent subsidence of the Venice Lagoon from continuous GPS and interferometric synthetic aperture radar, *Geochemistry geophysics geosystems*, vol. 13, Q07008, 8 PP doi:10.1029/2012GC004191

Canestrelli P, Mandich M, Pirazzoli PA, Tomasin A. 2001. '*Wind, depression and seiches: tidal perturbations in Venice (1951-2000)',* Città di Venezia, Centro Previsioni e Segnalazioni Maree, Comune di Venezia, 1-104.

Canestrelli P, Moretti F. 2004. I modelli statistici del comune di Venezia per la previsione della marea: valutazioni e confronti sul quinquennio 1997-2001. Atti dell'Istituto Veneto di Scienze Lettere ed Arti, Tomo CLXII, 479-516.

Canestrelli P, Pastore F. 2000. *Il Progetto Sistema Lagunare Veneziano*. Istituto Veneto di Scienze Lettere e Arti, Vol. II Tomo II, 635 - 663.

Cavaleri L, Bertotti L. 2004. Accuracy of the modelled wind and wave fields in encloses seas. *Tellus* 56A (2), 167-175.

De Zolt S, Lionello P, Malguzzi P, Nuhu A, Tomasin A. 2006. The disastrous storm of 4 November 1966 on Italy. *Nat. Hazards Earth Syst. Sci*. 6: 861–879.

Dee, D.P., Uppala, S.M., Simmons, A.J., Berrisford, P., Poli, P., Kobayashi, S., Andrae, U., Balmaseda, M.A., Balsamo, G., Bauer, P., Bechtold, P., Beljaars, A.C.M., van de Berg, L., Bidlot, J., Bormann, N., Delsol, C., Dragani, R., Fuentes, M., Geer, A.J., Haimberger, L., Healy, S.B., Hersbach, H., Hólm, E.V., Isaksen, L., Kållberg, P., Köhler, M., Matricardi, M., McNally, A.P., Monge-Sanz, B.M., Morcrette, J.-J., Park, B.-K., Peubey, C., de Rosnay, P., Tavolato, C., Thépaut, J.-N. and Vitart, F., 2011. The ERA-Interim reanalysis: configuration and performance of the data assimilation system . *Q.J.R. Meteorol. Soc*., 137:553-597, doi: 10.1002/qj.828.Motulsky, H. 1995. Intuitive Biostatistics, Oxford Univ. Press, pp 201-209.

Di Liberto T, Brian AC, Nickitas G, Blumberg AF, Taylor AA. 2011. Verification of a Multimodel Storm Surge Ensemble around New York City and Long Island for the Cool Season. *Wea. Forecasting*, 26: 922–939. doi: http://dx.doi.org/10.1175/WAF-D-10-05055.1

Eprim Y, Donato MD, Cecconi G. 2005. 'Gates strategies and storm surge forecasting system developed for the Venice flood management'. In *Fletcher C. and T.Spencer Eds., Venice and its lagoon*, State of Knowledge Cambridge University Press, Cambridge UK, 267-277.

Flowerdew J, Horsburgh K, Kevin C, Mylne K. 2009. Ensemble forecasting of storm surges. *Marine Geodesy*, 32 (2). 91-99. 10.1080/01490410902869151

Flowerdew J, Horsburgh K, Wilson C, Mylne K. 2010. Development and evaluation of an ensemble forecasting system for coastal storm surges. *Q. J. R. Meteorol. Soc.* 136: 1444–1456. DOI:10.1002/qj.648

Flowerdew J, Mylne K, Jones C, Titley H. 2012. Extending the forecast range of the UK storm surge ensemble. *Q. J. R. Meteorol. Soc*. DOI:10.1002/qj.1950

Hamill TM. 1997. Reliability diagrams for multicategory probabilistic forecasts. *Wea. Forecasting.* 12: 736–741.

Hazeleger, W., Severijns, C., Semmler, T., Stefanescu, S., Yang, S., Wang, X., Wyser, K., Dutra E., Baldasano, J.M., Bintanja, R., Bougeault, P., Caballero, R., Ekman, A.M.L., Christensen, J.H., van den Hurk, B., Jimenez, P., Jones, C., Kallberg, P., Koenigk, T., McGrath, R., Miranda, P., van Noije, T., Palmer, T., Parodi, J.A., Schmith, T., Selten, F., Storelvmo, T., Sterl, A., Tapamo, H., Vancoppenolle, M., Viterbo, P., Willen, U., 2010. EC-Earth: A Seamless Earth-System Prediction Approach in Action. *Bull Amer Meteor Soc* 91:1357-1363, doi: 10.1175/2010BAMS2877.1

Lionello P. , 2005. Extreme surges in the Gulf of Venice. Present and Future Climate in Fletcher C. and T. Spencer Eds., Venice and its lagoon, *State of Knowledge Cambridge University Press*, Cambridge UK, 59-65

Lionello, P. , 2012. The climate of the Venetian and North Adriatic region: Variability, trends and future change Phys. *Chem. Earth* 40-41:1-8

Lionello, P., Cavaleri, L., Nissen, K.M., Pino, C., Raicich, F., Ulbrich, U. 2012. Severe marine storms in the Northern Adriatic: Characteristics and trends, *Phys. Chem. Earth*, 40-41:93-105, DOI:10.1016/j.pce.2010.10.002

Lionello P., E.Elvini, A.Nizzero, 2003. A procedure for estimating wind waves and storm-surge climate scenarios in a regional basin: the Adriatic Sea case. *Clim. Research*., 23: 217-231

Lionello P., Galati, M.B., Elvini, E. 2012. Extreme storm surge and wind wave climate scenario simulations at the Venetian littoral, Phys. *Chem. Earth* 40-41, 86-92, DOI:10.1016/j.pce.2010.04.001

Lionello P, Mufato R, Tomasin A. 2005. Effect of sea level rise on the dynamics of free and forced oscillations of the Adriatic Sea. *Climate Research* 29: 23–39.

Lionello P, Sanna A, Elvini E, Mufato R. 2006. A data assimilation procedure for operational prediction of storm surge in the northern Adriatic Sea, *Continental shelf research* 26: 539-553.

Lionello P, Zampato L, Malguzzi P, Tomasin A, Bergamsco A. 1998. On the correct surface stress for the prediction of the wind wave field and the storm surge in the Northern Adriatic Sea, *Il nuovo Cimento* C21: 515-532.

Lorenz EN. 1965. A study of the predictability of a 28-variable atmospheric model. *Tellus*. 17: 321-333.

Massalin A, Zampato L, Papa A, Canestrelli P. 2007. Data monitoring and sea level forecasting in the Venice Lagoon: the ICPSM's activity, *Bollettino di Geofisica Teorica e Applicata*. 48: 241-257.

Molteni F, Buizza R, Palmer TN, Petroliagis T. 1996. The ECMWF Ensemble Prediction System: methodology and validation. *Q. J. R. Meteorol. Soc*. 122: 73–119.

Palmer TN, Molteni F, Mureau R, Buizza R, Chapelet P, Tribbia J. 1993. 'Ensemble prediction'. In *Proc. ECMWF Seminar (1992), ECMWF, Shinfield Park, Reading RG2 9AX, UK*.

Pérez-Muñuzuri, V., Lorenzo, M.N., Montero, P., Fraedrich, K., Kirk, E., Lunkeit, F., 2003. Response of a global atmospheric circulation model to spatio-temporal stochastic forcing: ensemble statistics, *Nonlinear Processes in Geophysics*, Vol. 10, 453-461.

Robinson AR, Tomasin A, Artegiani A. 1973. Flooding of Venice, phenomenology and prediction of the Adriatic storm surge. *Quarterly Journal of the Royal Meteorological Society*. 99 (422), 688-692.

Scarascia L. and Lionello P. , 2012. Global and regional factors contributing to the past and future sea level rise in the Adriatic Sea, submitted

Siek M, Solomatine DP. 2011. Optimized dynamic ensembles of multiple chaotic models in predicting storm surges. *Journal of Coastal Research*. 64: 1184 – 1188. Szczecin, Poland, ISSN 0749-0208

Talagrand O, Vautard R, Strauss B. 1997. 'Evaluation of probabilistic prediction systems'. In *Proceedings, ECMWF Workshop on Predictability (20−22 October 1997)*. Available from ECMWF, Shinfield Park, Reading,

Berkshire, England RG2 9AX. 1−26.

Tomasin A. 1972. Auto-regressive prediction of sea level in the northern Adriatic. *Rivista Italiana di Geofisica* XXI, 211–214.

Umgiesser G, Melaku Canu D, Cucco A, Solidoro C. 2004. A finite element model for the Venice Lagoon. Development, set up, calibration and validation. *Journal of Marine Systems*. 51: 123-145.

Zecchetto S, Cappa C. 2001. The spatial structure of the Mediterranean Sea winds revealed by ERS-1 scatterometer. *Int. J. Remote Sensing* 22: 1, 45–70.

Ziehmann C. 2001. Skill prediction of local weather forecasts based on the ECMWF ensemble. *Nonlinear Processes in Geophysics*. 8: 419-428.